nature cell biology

p38^{MAPK}/MK2-dependent phosphorylation controls cytotoxic RIPK1 signalling in inflammation and infection

Manoj B. Menon[1,3], Julia Gropengießer[2,3], Jessica Fischer[1], Lena Novikova[2], Anne Deuretzbacher[2,4], Juri Lafera[1], Hanna Schimmeck[2], Nicole Czymmeck[2], Natalia Ronkina[1], Alexey Kotlyarov[1], Martin Aepfelbacher[2], Matthias Gaestel[1,5] and Klaus Ruckdeschel[2,5]

Receptor-interacting protein kinase-1 (RIPK1), a master regulator of cell fate decisions, was identified as a direct substrate of MAPKAP kinase-2 (MK2) by phosphoproteomic screens using LPS-treated macrophages and stress-stimulated embryonic fibroblasts. p38^{MAPK}/MK2 interact with RIPK1 in a cytoplasmic complex and MK2 phosphorylates mouse RIPK1 at Ser321/336 in response to pro-inflammatory stimuli, such as TNF and LPS, and infection with the pathogen *Yersinia enterocolitica*. MK2 phosphorylation inhibits RIPK1 autophosphorylation, curtails RIPK1 integration into cytoplasmic cytotoxic complexes, and suppresses RIPK1-dependent apoptosis and necroptosis. In *Yersinia*-infected macrophages, RIPK1 phosphorylation by MK2 protects against infection-induced apoptosis, a process targeted by *Yersinia* outer protein P (YopP). YopP suppresses p38^{MAPK}/MK2 activation to increase *Yersinia*-driven apoptosis. Hence, MK2 phosphorylation of RIPK1 is a crucial checkpoint for cell fate in inflammation and infection that determines the outcome of bacteria–host cell interaction.

RIPK1 is a master regulator of cell fate under diverse cellular stress settings including cytokine-induced, chemical and metabolic stress[1,2]. It acts as a molecular switch that can elicit inflammation and cell survival, as well as apoptosis and necrosis[3]. This function is fulfilled by RIPK1 in canonical TNF receptor signalling, but also in infected host cells[4]. RIPK1 is engaged by the Toll-like receptors TLR3 and TLR4, which sense microbial double-stranded RNA and LPS, respectively[5,6]. The cytosolic TLR adapter TRIF relays the TLR3- and TLR4-derived signals to RIPK1. The activated downstream pathways overlap with canonical TNFR1 signalling. Thus, RIPK1 may signal inflammation and cell survival via TAK1/p38^{MAPK} and the IKK complex, or promote apoptosis through FADD and caspase-8 (CASP8). RIPK1 may also signal regulated necrosis, termed necroptosis, through RIPK3 interaction. The RIPK1 pro-survival function is independent of its enzymatic activity, whereas necroptosis requires RIPK1-kinase activity. RIPK1-dependent apoptosis displays stimulus- and context-specific requirement of its kinase activity[1,2,7,8].

RIPK1 activity is controlled by complex post-translational modifications, regulating the sequential formation of various RIPK1-containing multiprotein complexes. The non-degradative polyubiquitylation of RIPK1 in a membrane-bound pro-survival complex (complex I) enables recruitment of TAK1 and IKK in TNFR1-stimulated cells[9,10] leading to pro-survival gene expression. When pro-survival gene expression is impaired, a cytosolic pro-apoptotic complex consisting of TRADD, FADD and CASP8 is formed (complex IIa). RIPK1 is furthermore phosphorylated within complex I by IKK, resulting in inhibition of RIPK1-dependent cytotoxicity independent of gene transcription[11]. Under conditions that impair its ubiquitylation or phosphorylation by IKK, RIPK1 assembles with FADD and CASP8 into complex IIb to activate apoptosis. Following CASP8 or FADD inactivation, RIPK1 may trigger necroptosis by recruiting RIPK3 to the necrosome. RIPK1 undergoes autophosphorylation at several sites during apoptosis/necroptosis[12,13]. Furthermore, mutual RIPK1 and RIPK3 phosphorylation has been observed in the necrosome[12].

MAPKAP kinases 2/3 (MK2/3) are activated downstream of p38$^{MAPK}\alpha/\beta$ and are critical to transcriptional and post-transcriptional regulation of inflammation and the stress response[14,15]. MK2/3 regulate the transcription of a subset of immediate-early genes[16,17] and control cytokine messenger RNA translation

[1]Institute of Cell Biochemistry, Hannover Medical School, Hannover 30625, Germany. [2]Institute for Medical Microbiology, Virology and Hygiene, University Medical Center Eppendorf, Hamburg 20246, Germany. [3]These authors contributed equally to this work. [4]Present address: Department of Internal Medicine II, Division of Hematology, University Hospital of Würzburg, Würzburg 97080, Germany.
[5]Correspondence should be addressed to M.G. or K.R. (e-mail: gaestel.matthias@mh-hannover.de or k.ruckdeschel@uke.de)

Received 23 December 2016; accepted 15 August 2017; published online 18 September 2017; DOI: 10.1038/ncb3614

and stability by phosphorylating the mRNA-binding protein tristetraprolin (TTP)[18]. MK2 and MK2/3 deficiencies in mice result in an impaired inflammatory response with decreased LPS-induced TNF production and increased septic shock resistance[19,20]. MK2-deficient mice display impaired control of bacterial growth in a *Listeria* infection model[21]. A recent study demonstrated a negative role of $p38^{MAPK}$/MK2 signalling in Smac mimetic (SM)-induced TNF production, proposing $p38^{MAPK}$/MK2 co-inhibition as a treatment strategy for SM-resistant leukaemia[8].

Here, we identified RIPK1 as a direct substrate of MK2. RIPK1 is phosphorylated by MK2 in response to cell stress, LPS and TNF treatment, maintaining RIPK1 pro-survival functions in TNF-treated fibroblasts and LPS-stimulated macrophages cooperatively with IKK signalling. Hence, MK2 controls inflammation by increasing cytokine expression and inhibiting RIPK1-dependent cytotoxicity. This plays a role in combating bacterial infections, as demonstrated for the pathogen *Yersinia enterocolitica*, which targets pro-survival pathways including $p38^{MAPK}$/MK2 signalling to promote RIPK1-dependent apoptosis of infected macrophages.

RESULTS

Phosphoproteomics identified MK2-dependent RIPK1 phosphorylation

To identify downstream mediators of $p38^{MAPK}$/MK2 signalling and direct MK2 substrates, we used Phosphoscan, a motif antibody-based phosphoproteomic mass-spectrometric (MS) approach. MK2 belongs to the family of basophilic serine/threonine kinases with obligate requirement of an arginine at the −3 position of the phosphorylation site (Fig. 1a). Immortalized mouse embryonic fibroblast (MEF) and bone marrow-derived macrophage (BMDM) cell lines generated from MK2/3 double-deficient (DKO) mice[16,22] were rescued with retroviral-encoded MK2 or empty vector and stimulated with the stress-inducer anisomycin, or with LPS, respectively. Peptides from MEF and BMDM lysates were immunoprecipitated with anti-phospho-PKD substrate motif (pPKD-motif) antibody or with an anti-basophilic motif antibody cocktail, respectively. Label-free quantitative LC/MS–MS analysis identified MK2-dependent phosphorylation events at proteins involved in different biological processes (Supplementary Fig. 1a). One specific target, which was consistently and significantly phosphorylated in a MK2-dependent manner, was the serine/threonine kinase RIPK1. Phosphopeptides corresponding to RIPK1 residues Ser313 and Ser336 were strongly enriched in MK2-rescued MEFs and BMDMs (Fig. 1b and Supplementary Fig. 1b). While Ser313 is a potential, proline-directed $p38^{MAPK}$ target that is not conserved in human RIPK1 and not part of a basophilic motif, sequence analysis revealed an additional consensus MK2-target motif at Ser321 (Fig. 1c). To check whether Ser321 is a potential target site for MK2, we monitored stress-induced GST-RIPK1 phosphorylation in HEK293T cells by pulldown and MS analysis. Several residues on RIPK1, including Ser321, were identified as phosphorylated, suggesting these residues as possible MK2-target sites (Supplementary Figs 1c,d). Murine RIPK1 Ser321 and Ser336 are conserved across mammals (corresponding to Ser320 and Ser335 in hRIPK1) and are located in the intermediate domain close to the CASP8 cleavage site Asp325 (Asp324 in hRIPK1) and the major Lys63-ubiquitylation site Lys376 (Lys377 in hRIPK1) (Fig. 1c).

MK2 directly phosphorylates murine RIPK1 at Ser321 and Ser336

To verify the $p38^{MAPK}$/MK2-dependent phosphorylation sites on RIPK1, we mutated the respective serines and analysed them by probing with pPKD-motif antibodies. When RIPK1 wild type (WT) or phosphorylation site mutants (S321A, S336A) were expressed as GST-fusion proteins in HEK293T cells and enriched by GST-pulldown, a reduction in the stress-induced phosphorylation was noticed for both mutants (Fig. 1d). The observed phosphorylation was sensitive to treatment with the $p38^{MAPK}$ inhibitor BIRB796. HSPB1, a *bona fide* substrate of MK2, was used as control. *In vitro* kinase assays with recombinant GST-RIPK1-ΔC (1–500aa) and recombinant MK2 activated by $p38^{MAPK}$ *in vitro* (Fig. 1e) showed prominent phosphorylation of GST-RIPK1-ΔC (1–500aa) by MK2 (but not by $p38^{MAPK}$ alone). Phosphorylation events were still observed for the single-phosphorylation-site mutants S321A and S336A, but were almost completely suppressed for the double mutant S321A/S336A (SS/AA). Mutation of the potential $p38^{MAPK}$ target site Ser313 had no major impact on stress-induced RIPK1 phosphorylation (Supplementary Fig. 1e). Thus, Ser321 and Ser336 are the major RIPK1-phosphorylation sites for MK2, whereas $p38^{MAPK}$ seems less relevant.

Stress- and cytokine-induced RIPK1 phosphorylation is $p38^{MAPK}$/MK2-dependent and independent of RIPK1-kinase activity

Immunoprecipitation experiments with pPKD-motif antibodies enriched RIPK1 specifically from MK2-rescued DKO MEFs, confirming MK2-dependent RIPK1 phosphorylation similar to HSPB1 (Fig. 2a). Similar to previously characterized MK2 substrates[23,24], wild-type RIPK1 overexpression in HEK293T cells led to spontaneous phosphorylation and a band shift, which was abrogated by the $p38^{MAPK}$ inhibitor BIRB796 or by mutation of either Ser321 or Ser336, while a catalytic dead RIPK1 mutant (D138N) showed a double band pattern similar to that of wild-type RIPK1 (Fig. 2b). A phosphorylation-induced band shift of RIPK1 after TNF stimulation has previously been attributed to its autophosphorylation activity[25]. TNF stimulation generated slow migrating RIPK1 bands; however, the appearance of these shifted bands was inhibited by BIRB796 pretreatment, but not by Necrostatin-1 (Nec-1, Fig. 2c), an efficient and specific RIPK1-kinase inhibitor[13], even at high concentration (Supplementary Fig. 1f). A specific IKKβ-inhibitor also did not affect this RIPK1 band shift (Supplementary Fig. 1g). When GST-RIPK1 was enriched from anisomycin-stimulated cells and probed by pPKD-motif antibody, strong signals were detected. These signals were again abrogated by BIRB796 with a downshift of the RIPK1 band (Fig. 2d), confirming that $p38^{MAPK}$/MK2-mediated phosphorylation is responsible for reduced RIPK1 electrophoretic mobility. Two RIPK1-kinase-inactive mutants (D138N and K45R) showed strong phosphorylation and upshifted bands, ruling out RIPK1-kinase activity requirement for the observed shift (Fig. 2d). MK2 activity involvement in RIPK1 phosphorylation was further verified using catalytic dead and constitutively active MK2 mutants in the GST-enrichment assays (Fig. 2e). Co-expression of constitutively active MK2-TT/EE was sufficient to mediate strong phosphorylation and a shift of catalytic dead RIPK1-D138N even in the presence of BIRB796, whereas catalytic

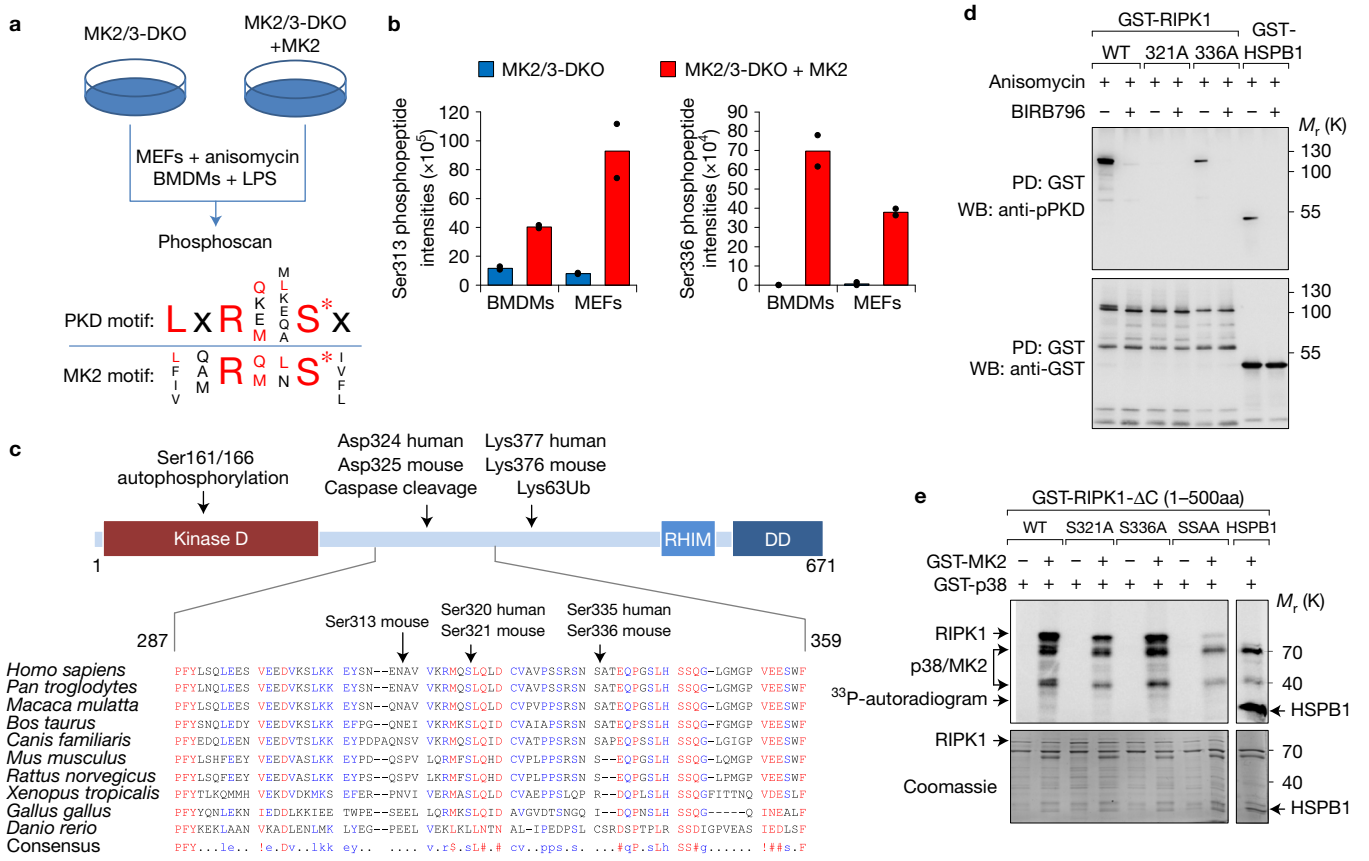

Figure 1 Identification of RIPK1 as a substrate of MK2 by two different phosphoproteomic approaches. (**a**) Schematic representation of the phosphoproteomic approach (Phosphoscan) and the phosphorylation-motif consensus between MK2 and the pPKD-motif antibody used in the screen. (**b**) Label-free quantification data for two RIPK1-derived phosphopeptides (Ser313 and Ser336) discovered in both macrophages and MEFs. The data points indicate values from two separate LC–MS injections. (**c**) Domain organization of RIPK1 showing the conserved phosphosites and additional residues of functional significance. (**d**) Ser321/Ser336 constitute the major stress-induced p38-dependent phosphorylation sites of mRIPK1, as detected by western blotting with pPKD-motif antibody (anti-pPKD), after GST-pulldown from transfected HEK293T cells. PD, pulldown. (**e**) Bacterially purified, recombinant mRIPK1 (1–500aa) is a direct substrate of MK2, *in vitro* activated by p38. p38 does not phosphorylate RIPK1 and MK2-mediated RIPK1 phosphorylation is abrogated by S321A/S336A mutagenesis. The MK2 substrate HSPB1 is shown as a positive control in **d** and **e**. The samples in the spliced panel (**e**) were obtained and processed simultaneously. Unprocessed original scans of blots are shown in Supplementary Fig. 7. Results shown are representative of four (**d**) and two (**e**) independent experiments, respectively.

dead MK2-K79R diminished the stress-induced RIPK1 phosphorylation (Fig. 2e). Likewise, the anisomycin-induced endogenous RIPK1 band shift in MK2/3-DKO MEFs was restored by wild-type MK2 but not by MK2-K79R (Fig. 2f), showing that MK2 catalytic activity is indispensable for the observed RIPK1 phosphorylation. Similarly, when RIPK1, RIPK1-D138N and RIPK1-SSAA were expressed in RIPK1-deficient Jurkat cells, WT and catalytic dead RIPK1 displayed a shift, whereas the phosphorylation site mutant did not (Fig. 2g). MK3 expression could also rescue RIPK1 phosphorylation (Supplementary Fig. 1h).

p38^{MAPK} and MK2 associate with RIPK1 in cytoplasmic complexes

To test MK2 involvement in RIPK1-associated complex assembly, we assessed MK2 and RIPK1 interaction in co-immunoprecipitation and pulldown assays. MK2 efficiently precipitated co-expressed Myc-tagged RIPK1 (Fig. 3a) and specifically enriched endogenous RIPK1 from transfected HEK293T cells (Fig. 3b), suggesting a strong interaction between these proteins independent of stimulation. Pull-downs with two RIPK1 carboxy-terminal truncations lacking the death domain (RIPK1 (1–588aa)), or lacking both the death and RHIM domains (RIPK1 (1–500aa)), suggested that the region containing amino acids 500–588 harbouring the RHIM domain is necessary for MK2 binding (Fig. 3c). Surprisingly, RHIM motif mutation (^{528}IQIG^{531}/AAAA)[26] did not interfere with RIPK1–MK2 interaction (Fig. 3d). There is a strong correlation between the self-interacting capabilities of RIPK1 mutants and their abilities to recruit MK2 (Fig. 3c,d and Supplementary Fig. 2a–d). The RIPK1 (1–588aa) mutant failed to interact with MK2 following RHIM motif mutation (Supplementary Fig. 2c), suggesting that RIPK1 dimerization via either of the two self-associating domains (death or RHIM domain) could facilitate the interaction with MK2. However, strong association of RIPK1 with MK2 appears dispensable for Ser321/Ser336 phosphorylation, as RIPK1 (1–500aa) was efficiently phosphorylated by MK2 *in vitro* and *in vivo* (Figs 1e and 2d). The MK2-pulldown also enriched p38^{MAPK} and the ubiquitin-binding adapter p62. While p38 binding

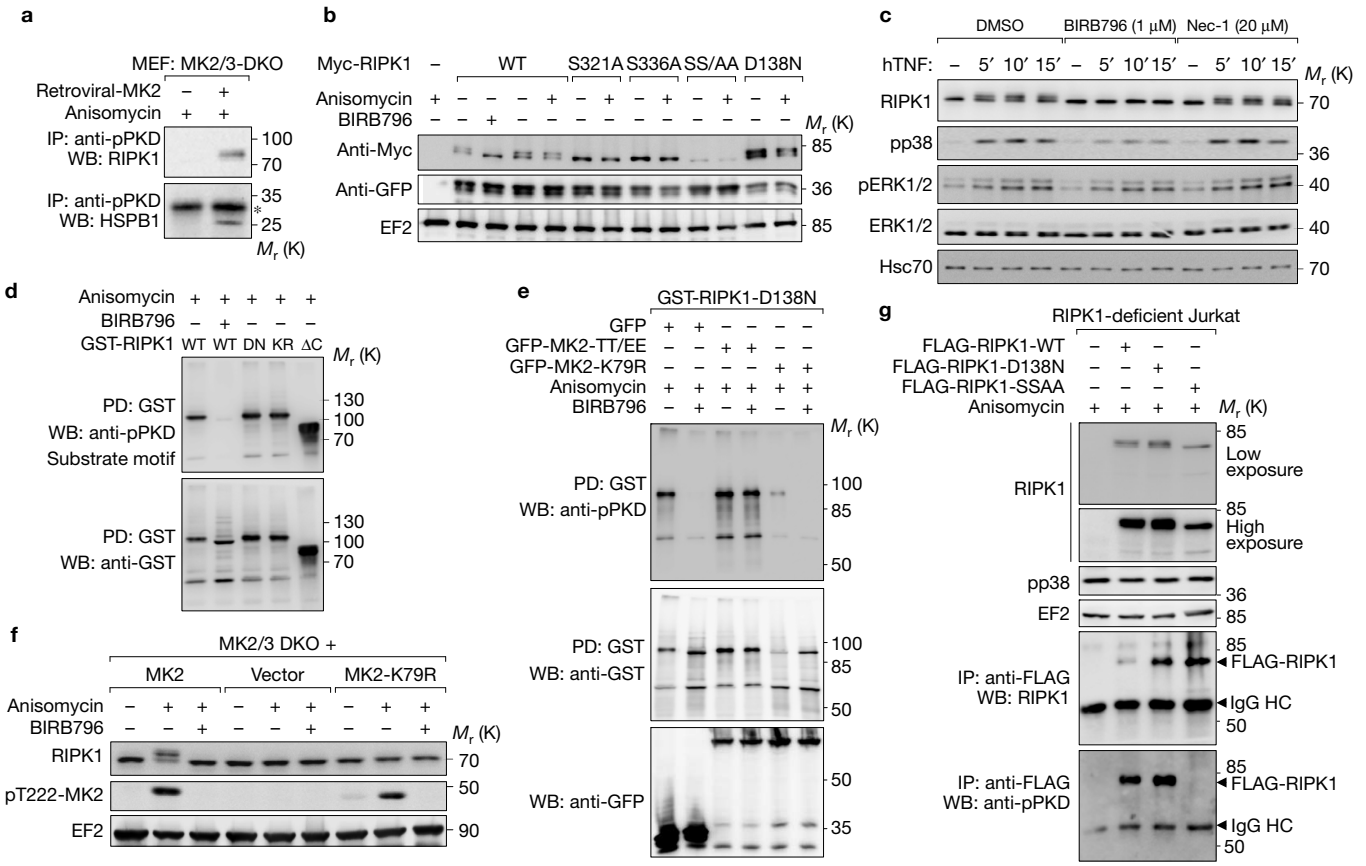

Figure 2 p38/MK2-dependent RIPK1 phosphorylation depends on the catalytic activity of MK2 but is independent of the RIPK1-kinase activity. (**a**) Endogenous phosphoproteins were immunoprecipitated from lysates of MK2/3-DKO and retrovirally rescued MEFs using pPKD-motif antibody and IPs were probed with RIPK1 and HSPB1 antibodies (the asterisk denotes the light chain of immunoprecipitating IgG). (**b**) HEK293T cells transfected with GFP-expression vector and the indicated plasmid constructs expressing Myc-tagged RIPK1 were stimulated with anisomycin with or without pretreatment with the $p38^{MAPK}$ inhibitor BIRB796. Electrophoretic mobility shifts of RIPK1 were monitored by western blotting with anti-Myc antibodies. The blot was probed with anti-GFP and anti-EF2 antibodies as transfection and loading controls. (**c**) WT-MEF cells were treated as indicated with BIRB796 or RIPK1 inhibitor Necrostatin-1 (Nec-1), followed by TNF stimulation. Samples were subjected to western blotting with the indicated antibodies. Hsc70 is shown as a loading control. (**d**) GST-tagged RIPK1-expression vectors encoding wild-type (WT), 1–500aa (ΔC), or the catalytic dead mutants D138N (DN) or K45R (KR) were transfected in HEK293T cells, treated as indicated and lysates were subjected to GST-pulldown and probed with pPKD-motif antibody. Anti-GST signals are shown as controls. PD, pulldown. (**e**) HEK29T cells were transfected with indicated plasmids and subjected to phospho-immunoblotting as above. (**f**) MK2/3-DKO MEF cells transduced with empty vector, WT-MK2 or a catalytic dead mutant MK2 (K79R) were treated as indicated and immunoblotted for RIPK1. (**g**) RIPK1-deficient Jurkat cells were rescued with lentiviral vectors expressing FLAG-tagged WT, D138N (catalytic dead) or S321A/S336A (SSAA) mutant RIPK1. Lysates from anisomycin-stimulated cells were subjected to anti-FLAG-IP and probed as indicated after western blotting. The phosphorylation and the band shift of RIPK1 is dependent on Ser321/Ser336 and independent of the RIPK1 catalytic activity. Unprocessed original scans of blots are shown in Supplementary Fig. 7. Results shown are representative of two (**a**,**c**,**g**) and three (**b**,**d**,**f**) independent experiments, respectively. The experiment in **e** was performed once.

was independent of RIPK1 co-expression, the RIPK1-interactor p62 (ref. 27) was recruited to MK2 in a RIPK1-dependent manner. In the presence of full-length RIPK1, MK2 co-precipitated CASP8, FADD and cFLIP (Fig. 3c). Thus, MK2 and $p38^{MAPK}$ can associate with a cytoplasmic complex reminiscent of an immature ripoptosome via interaction with RIPK1 (Fig. 3f)[28,29]. This pre-ripoptosome may become activated to elicit apoptosis or necroptosis depending on the composition of its core components.

To define the RIPK1-interacting region in MK2, we used two C-terminal truncations lacking the regulatory C terminus and the catalytic core subdomains IX–XI (GFP-MK2 (1–223aa)), or V–XI (GFP-MK2 (1–132aa)), respectively. GST-pulldown assays with RIPK1 (1–588aa) demonstrated that the catalytic subdomains I–IV in GFP-MK2 (1–132aa) are sufficient for RIPK1 binding (Fig. 3e). This region does not overlap with the C-terminal $p38^{MAPK}$-binding site and, similar to binding of MK2 to Edr2 (ref. 30), could allow formation of a ternary complex consisting of RIPK1, MK2 and $p38^{MAPK}$ (Fig. 3f).

As RIPK3 is necessary for RIPK1 phosphorylation[12], we asked whether RIPK3 regulates RIPK1 phosphorylation via MK2 recruitment. Whereas GST-MK2 efficiently co-purified RIPK1 in a GST-pulldown assay, there was only weak RIPK3 enrichment, indicating that RIPK3 does not directly interact with MK2 (Supplementary Fig. 2e). However, MK2, RIPK1 and RIPK3 co-expression led to significant co-purification of RIPK3, suggesting a trimeric complex wherein RIPK1 could bridge the MK2 and RIPK3 interaction (Supplementary Fig. 2e).

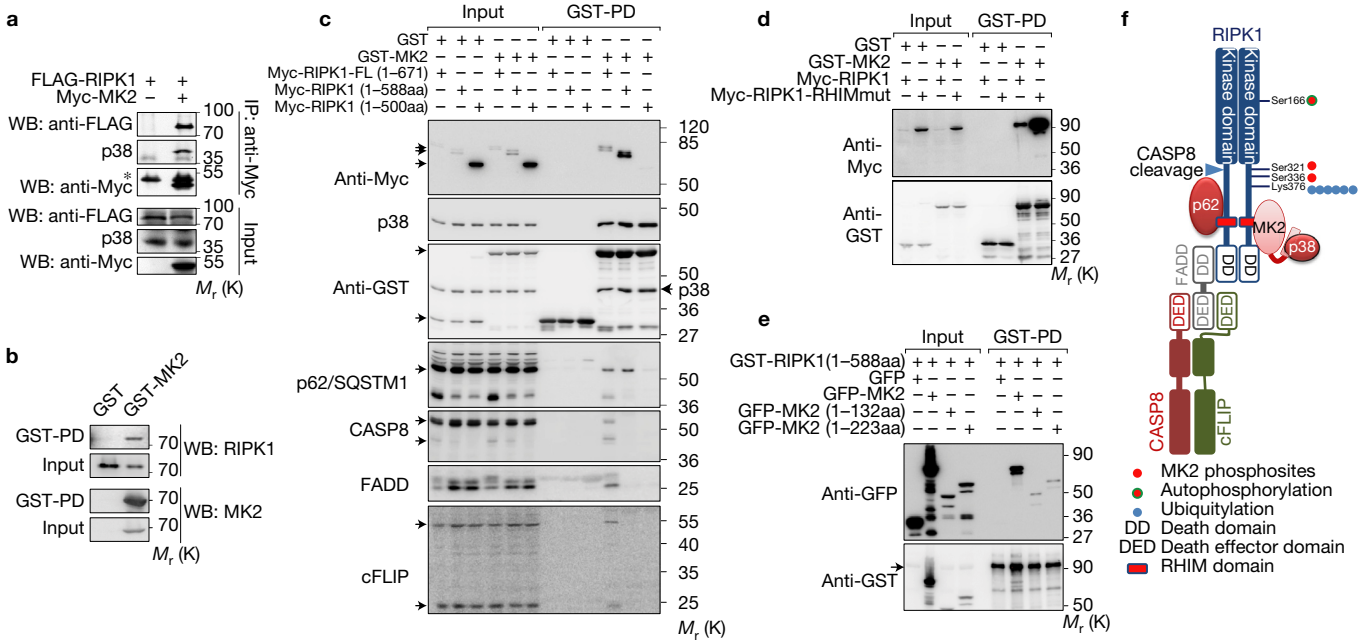

Figure 3 MK2 is part of a RIPK1-comprising complex. (**a**) RIPK1 co-immunoprecipitates with MK2. HEK293 cells were co-transfected with expression plasmids for FLAG-hRIPK1, and either Myc-MK2 or empty vector (–). Myc-MK2 was immunoprecipitated, and co-precipitation of FLAG-RIPK1 and endogenous p38 was analysed by immunoblotting (the asterisk denotes the heavy chain of immunoprecipitating IgG). Expression of FLAG-RIPK1, Myc-MK2 and p38 was controlled in cellular lysates. (**b**) GST-MK2-pulldown (PD) co-precipitates endogenous RIPK1 from transfected HEK293T cells. (**c**) Empty GST or GST-MK2 expression vectors were co-transfected with the indicated full-length (FL) or truncated mRIPK1 expression vectors. GST-pulldowns and input controls were probed with the indicated antibodies to detect additional endogenous interaction partners. (**d**) RIPK1 with a mutated RHIM domain efficiently interacts with MK2. (**e**) The amino-terminal 132 amino acids of MK2 are sufficient to enrich GST-RIPK1 (1–588aa), as determined by GST-MK2-pulldown from transfected HEK 293T lysates. (**f**) Schematic presentation of the multiprotein complex consisting of dimerized RIPK1, MK2/p38, p62, CASP8, FADD and cFLIP. Unprocessed original scans of blots are shown in Supplementary Fig. 7. Results shown are representative of two (**a**–**c**,**e**) and three (**d**) independent experiments, respectively.

MK2 and IKK suppress TNF-induced RIPK1 autophosphorylation, apoptosis and necroptosis

To detect functional consequences of MK2-dependent RIPK1 phosphorylation, we monitored TNF-induced death of MK2-deficient MEFs rescued with MK2 or empty vector control. As IKK directly phosphorylates RIPK1 to inhibit its cytotoxic potential in TNF-stimulated cells[11], we analysed MK2-dependent cell death in the presence and absence of the IKKβ inhibitor BMS-345541 (BMS). TNF induced cell death in the presence of BMS (apoptosis) and a stronger necroptotic response following co-treatment with the pan-caspase inhibitor zVAD (Fig. 4a–c and Supplementary Fig. 3a). MK2-deficiency strongly sensitized cells to both apoptosis and necroptosis, indicating MK2-dependent death suppression. Given that BMS/zVAD-mediated necroptosis (Fig. 4b) and BMS-mediated apoptosis (Supplementary Fig. 3a) were inhibited by Nec-1, it is likely that the MK2-dependent cell death suppression proceeds via RIPK1. Treatment with inhibitors for MK2 (PF3644022, PF) and IKK led to an additive cytotoxic effect of both inhibitors in TNF/zVAD-induced necroptosis, suggesting cytoprotective functions of both IKK and MK2 (Fig. 4c). We also detected an additive effect of MK2 deficiency and IKK inhibition on RIPK1-Ser166 autophosphorylation[31] (Fig. 4d). Although the functional significance of pSer166 is not yet defined, there is evidence that RIPK1 autophosphorylation correlates with induction of its kinase activity and cytotoxic RIPK1 complex formation[3,4,32]. This suggests that inactivation of both RIPK1-phosphorylating kinases (MK2 and IKK) is required for complete induction of the cytotoxic RIPK1 activity. The importance of MK2 signalling in RIPK1-dependent cell death suppression was also observed when TNF+SM were used as cytotoxic stimuli (Supplementary Figs 3b,c). To test whether RIPK1 double phosphorylation at Ser321/Ser336 could protect cells from TNF-induced death, we reconstituted RIPK1-knockout MEFs (RIPK1 KO) with either wild-type RIPK1 (RIPK1-WT) or a RIPK1 mutant in which Ser321 and Ser336 were replaced by alanine (RIPK1-SSAA). Importantly, TNF/BMS-induced apoptosis was significantly enhanced in RIPK1-SSAA-transduced cells compared with RIPK1-WT MEFs (Fig. 4e). This increase in cell death was significantly, but not completely suppressed by Nec-1s, probably due to increased RIPK1-independent death in a fraction of cells with diminished RIPK1 expression (Supplementary Fig. 3d). Enhanced death was also evident in the Nec-1s-sensitive fraction of dying cells expressing the RIPK1-SSAA mutation (Supplementary Fig. 3e). Furthermore, a kinase-inactivating mutation (RIPK1-SSAA-K45A) substantially protected against cell death under these conditions (Supplementary Fig. 3f), reinforcing RIPK1 involvement. RIPK1-SSAA-expressing cells also showed constitutively high RIPK1 autophosphorylation as monitored by phospho-Ser166 immunoblotting (Fig. 4f) and *in vitro* kinase assay (Supplementary Fig. 3g). Consistent with a recently suggested role of cytosolic RIPK1 ubiquitylation in subsequent autophosphorylation and necrosome activation[33], the RIPK1-SSAA mutant also showed enhanced

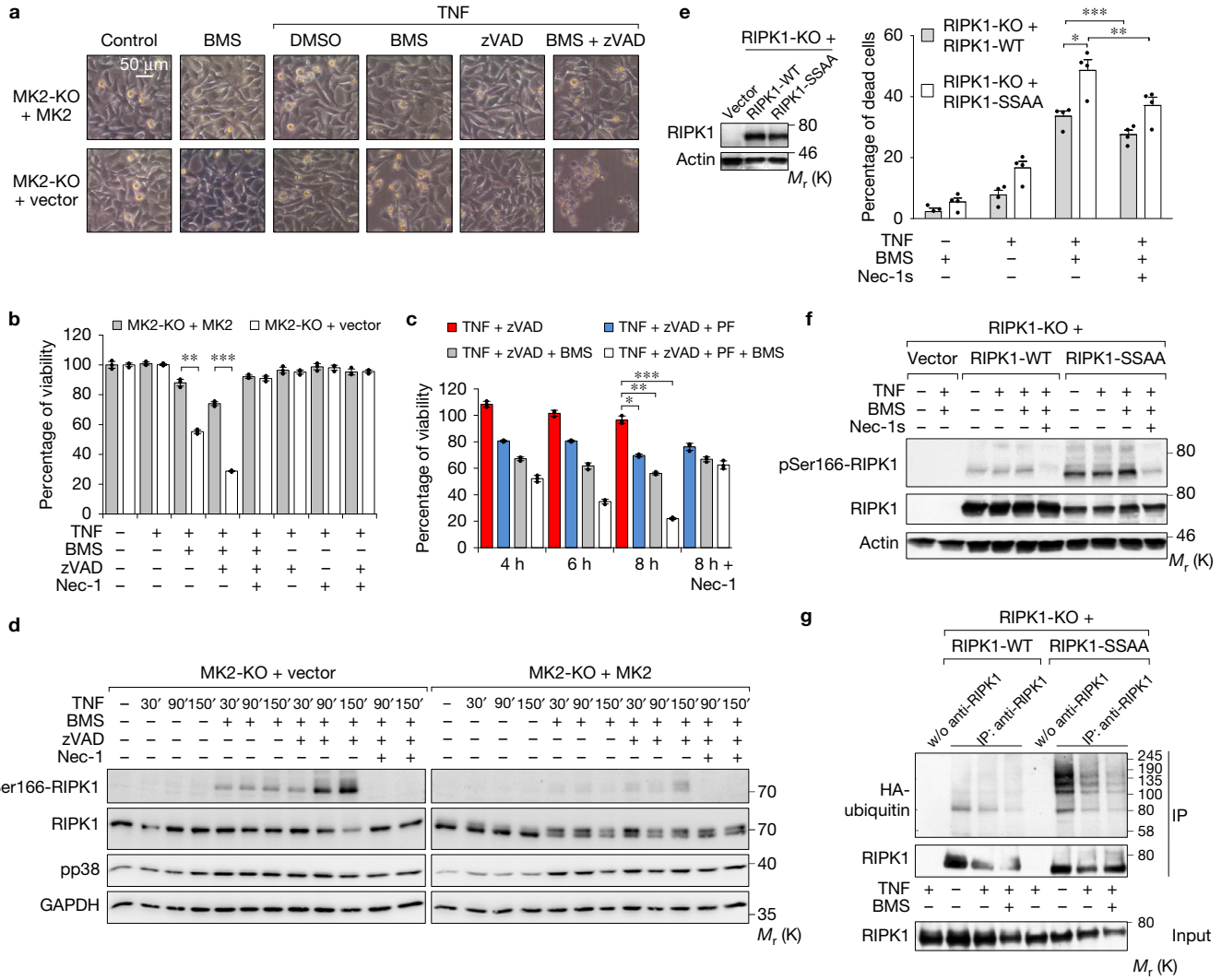

Figure 4 MK2-dependent RIPK1 phosphorylation suppresses TNF-mediated apoptosis and necroptosis and RIPK1 autophosphorylation. (**a**) MK2-KO MEFs transduced with retroviral MK2-expressing or control vector were treated as indicated for 3 h and images were acquired. (**b**) MK2-KO and rescued MEFs were treated as indicated for 5 h and cell viability was assessed by WST-1 assay. Average values of $n=3$ independent wells are plotted ± s.d. ($^{**}P=0.00028$; $^{***}P=0.00017$). (**c**) MK2-rescued cells were treated as indicated and cell viability data are presented as in **b** (average values of $n=3$ independent wells ± s.d.; $^{*}P=0.0016$; $^{**}P=0.0006$; $^{***}P=0.0002$). (**d**) MK2-KO and rescued MEFs were stimulated with TNF in combination with BMS or Nec-1 and lysates were immunoblotted with indicated antibodies. (**e**) RIPK1-KO MEFs were lentivirally transduced with vectors for empty control (vector), RIPK1-WT or RIPK1-S321A/S336A (RIPK1-SSAA) mutant. The cells stably selected with puromycin were treated as indicated for 21 h and cell death was assessed by Sytox Green nucleic acid stain. Quantitative results are expressed as means ± s.e.m. from $n=4$ independent experiments ($^{*}P=0.008$; $^{**}P=0.0393$; $^{***}P=0.0352$) (right). The RIPK1 protein levels were analysed by immunoblotting and equal loading was controlled by determining the actin levels (left). (**f**) Western blot detection of pSer166-RIPK1 in cells transduced as in **e** and stimulated with TNF for 1.5 h. The total pools of RIPK1 were controlled by stripping and re-probing the membrane with antibodies against RIPK1. Anti-actin was used as loading control. (**g**) The cells indicated in **f** were transfected with HA-ubiquitin, stimulated the next day as indicated for 2.5 h, and analysed by RIPK1-IP and immunoblotting with anti-HA antibodies. IPs without RIPK1 antibody served as control. The total pools of RIPK1 were analysed in the cell lysates (input). Statistical analysis was performed using two-tailed unpaired *t*-test. Viability data shown in **b**,**c** are representative of three independent experiments. Statistical source data and results of independent repeat experiments are provided in Supplementary Table 1. Shown immunoblot results are representative of two (**g**) or three (**a**,**d**) or four (**f**) independent experiments. Unprocessed original scans of blots are shown in Supplementary Fig. 7.

constitutive ubiquitylation (Fig. 4g). Thus, the MK2-mediated Ser321/Ser336-RIPK1 phosphorylation may negatively regulate its death-promoting potential by modulating the interplay between ubiquitylation and autophosphorylation in cytotoxic complexes. However, the potential phosphomimicking mutant RIPK1-S321D/S336D, which was protective in cytotoxicity assays (Supplementary Figs 3h,i), also displayed constitutive autophosphorylation at Ser166.

RIPK1 phosphorylation by MK2 proceeds in response to diverse pro-inflammatory stimuli and bacterial infection

We analysed endogenous RIPK1 phosphorylation by MK2 in MEFs in response to TNF and IL-1 treatment and detected the MK2-dependent band shift of RIPK1 after 5–30 min only in MK2-harbouring cells (Fig. 5a,b). There was no significant effect of MK2 on NFκB activation, as assessed by monitoring IκBα phosphorylation. Consistently, we

did not observe significant differences in RIPK1 recruitment and ubiquitylation in the TNFR-associated complex enriched by FLAG-tagged TNF (Supplementary Fig. 3j). MK2 was not detectable in the TNFR immunoprecipitates (Supplementary Fig. 3j). A major fraction of RIPK1 and MK2 was cytosolic, independent of stimulation (Fig. 5c). There was also no preferential membrane localization of phosphorylated RIPK1, suggesting that MK2 phosphorylates RIPK1 in the cytosol. The MK2 phosphorylation-specific band shift of RIPK1 was also detected only in MK2-rescued LPS-stimulated macrophages (Fig. 5d). Co-immunoprecipitation of MK2 with RIPK1 revealed that MK2 interacts with cytosolic RIPK1 in macrophages (Fig. 5e). Short-term LPS stimulation had no influence on the fraction of RIPK1 complexed with MK2. Pharmacological MK2 inactivation increased and stabilized MK2 association with RIPK1, although the interaction decreased following prolonged LPS stimulation (Fig. 5e, LPS 90′). Additional IKK blockade did not further influence MK2 binding. Macrophage infection with the Gram-negative bacterial pathogen *Yersinia enterocolitica* (Ye) also led to strong RIPK1 phosphorylation (Fig. 5f). Whereas infection with a strain lacking *Yersinia* outer protein YopP (Ye-Δ*yopP*) triggered robust RIPK1 phosphorylation almost indistinguishable from LPS stimulation, the RIPK1 phosphorylation induced by the Ye wild-type strain was downregulated within 40–60 min (Fig. 5f). The RIPK1 phosphorylation events triggered by both *Yersinia* strains proceeded only in MK2-harbouring cells, indicating $p38^{MAPK}$/MK2 stimulation and RIPK1 phosphorylation by MK2 in response to bacterial infection (Fig. 5g).

YopP triggers RIPK1-dependent macrophage apoptosis

To test the response of bacteria-infected macrophages we investigated *Yersinia*-induced apoptosis. Pathogenic *Yersinia* species utilize a type-III-protein secretion system to inject virulence-associated Yops into host cells[34]. YopP in *Y. enterocolitica* (denoted YopJ in *Y. pestis* and *Y. pseudotuberculosis*) elicits apoptosis in macrophages. We compared WT and RIPK1-deficient mouse fetal liver macrophages in *Yersinia*-induced apoptosis. Whereas the Ye WT strain triggered massive RIPK1-dependent apoptosis, the YopP-deficient strain Ye-Δ*yopP* displayed weak cytotoxicity (Fig. 6a). There were no differences in the death rates for both *Yersinia* strains in RIPK1-deficient cells, indicating that RIPK1 mediates the cell death-conferring effect of YopP. Similar observations were made for the macrophage cell line J774A.1 following RIPK1 short hairpin RNA (shRNA)-mediated knockdown (Supplementary Fig. 4a). Active CASP8 p18 levels (Fig. 6b) and executioner caspase-3 activity (Fig. 6c) indicated that apoptosis constitutes the major YopP- and RIPK1-dependent cell death mechanism. In contrast, RIPK1-independent death of Ye- and Ye-Δ*yopP*-infected RIPK1-deficient cells is attributable to caspase-independent necrosis because caspase-3 activity was moderate and the RIPK3/necroptosis inhibitor GSK'872 prevented cytotoxicity (Fig. 6d).

YopP represses signalling to TAK1, IKKβ and $p38^{MAPK}$/MK2 in infected macrophages

We hypothesized that the YopP pro-apoptotic effect in macrophages may involve inhibition of $p38^{MAPK}$/MK2 signalling. The $p38^{MAPK}$/MK2-dependent RIPK1 phosphorylation was rapidly downregulated by WT *Yersinia*, whereas the phosphorylation only slowly declined after stimulation with YopP-negative Ye-Δ*yopP* or with LPS (Fig. 5f). This RIPK1 phosphorylation was independent of RIPK1-kinase activity (Supplementary Figs 4b,c) and TNFR1 signalling (Supplementary Fig. 4d). Furthermore, TNFR1 was not required for *Yersinia*-induced cell death (Supplementary Fig. 4e). Thus, YopP may downregulate RIPK1 phosphorylation by directly inhibiting pathways that mediate $p38^{MAPK}$/MK2 activation. YopP/YopJ acts as an acetyltransferase on critical residues in the activation loops of the upstream MAP3K of $p38^{MAPK}$, TAK1, as well as of IKKβ and the MAP2K family[35–37]. Infection with Ye-Δ*yopP* triggered strong induction of the regulatory TAK1 phosphorylation after 90 min, whereas YopP presence in the WT strain Ye inhibited this phosphorylation (Fig. 6e). Similar results were obtained for IKKβ (Fig. 6e), indicating that YopP may target both pathways involved in RIPK1 phosphorylation. Importantly, $p38^{MAPK}$ activation was also suppressed by WT Ye after 60 min (Fig. 6f), which was accompanied by downregulation of the RIPK1 band shift. YopP may inhibit $p38^{MAPK}$/MK2 through the blockade of upstream TAK1. In fact, TAK1 inhibitors suppressed $p38^{MAPK}$/MK2-mediated RIPK1 phosphorylation almost as efficiently as p38/MK2 inhibitors (Supplementary Fig. 4f). Thus, TAK1 acetylation and downstream signalling inhibition could account for the YopP pro-apoptotic effect. TAK1 or IKK inhibition promoted RIPK1-dependent apoptosis of Ye-Δ*yopP*-infected or LPS-stimulated macrophages (Supplementary Fig. 4g–j), indicating anti-apoptotic TAK1 and IKK activities in bacteria-infected macrophages. Apoptosis conferred by Ye-Δ*yopP* or LPS in these conditions required RIPK1-kinase activity (Supplementary Fig. 4h).

$p38^{MAPK}$/MK2 and IKKβ cooperatively restrict RIPK1-dependent apoptosis of macrophages

We wondered how the reduced phosphorylation of RIPK1 by MK2 after *Yersinia* infection relates to macrophage sensitivity to apoptosis. We compared *Yersinia*-mediated cell death in RIPK1-phosphorylation-competent (MK2-rescued) versus -incompetent macrophages (MK2/MK3-deficient DKO). As expected, the WT *Yersinia* strain Ye rapidly triggered death in MK2-positive as well as MK2-deficient macrophages (Fig. 6g). Nec-1s treatment significantly reduced cell death in both lines, indicating that Ye, which inhibits MK2-dependent RIPK1 phosphorylation, engages the RIPK1-kinase activity for apoptosis initiation. To evaluate a link between the $p38^{MAPK}$/MK2-dependent phosphorylation status of RIPK1 and *Yersinia*-mediated apoptosis, we infected the cells with the YopP-negative strain Ye-Δ*yopP* in the presence or absence of inhibitors for $p38^{MAPK}$ (SB203580, SB) or MK2 (PF3644022, PF). The application of SB or PF, but not of inhibitors for JNK (SP600125) or MEK1 (PD098059), mimicked the inhibitory effect of YopP on the $p38^{MAPK}$/MK2 pathway and suppressed RIPK1 phosphorylation triggered by Ye-Δ*yopP* (Supplementary Fig. 4f). Ye-Δ*yopP* infection, similar to LPS treatment (Supplementary Fig. 5a), only modestly induced death in MK2-positive macrophages (Fig. 6g). Cell death levels mediated by Ye-Δ*yopP* and LPS were slightly augmented by SB, by PF or during infection of MK2-deficient cells. In both conditions, Nec-1s dampened the cytotoxic response (Fig. 6h) but the effects were not reliably significant. Thus, $p38^{MAPK}$/MK2 blockade alone triggers only a moderate level of apoptosis in Ye-Δ*yopP*- or LPS-stimulated macrophages.

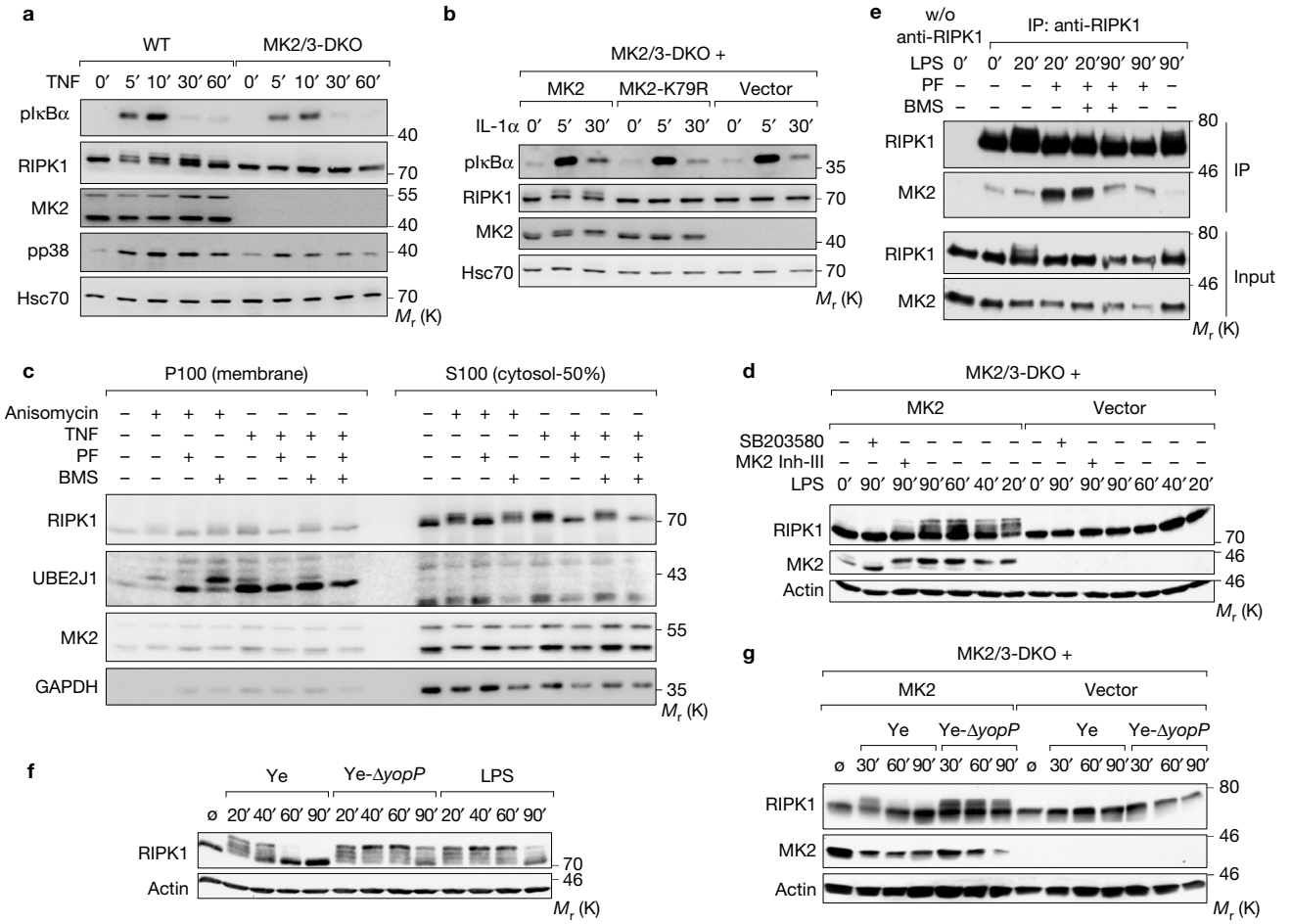

Figure 5 Diverse pro-inflammatory stimuli and *Yersinia* infection induce MK2-dependent RIPK1 phosphorylation in the cytosol. (**a**) Immortalized MEFs from WT and MK2/3-DKO mice were stimulated with recombinant hTNF for the indicated times and cell lysates were subjected to western blot analysis. (**b**) Immortalized MK2/3-DKO MEFs transduced with empty vector (vector), WT-MK2 (MK2) or catalytic dead MK2 (MK2-K79R) expression vectors were treated with IL-1α for the indicated time points and lysates were analysed for RIPK1 and IκB phosphorylation. MK2 and Hsc70 are shown as controls. (**c**) Membrane (P100) and cytosolic (S100) fractions from WT immortalized MEFs prepared as described in the Methods were subjected to immunoblotting to verify RIPK1, pRIPK1 (shifted-band) and MK2 localization. UBE2J1, a membrane localized protein, and GAPDH, a cytoplasmic protein, are shown as controls. (**d**) RIPK1 electrophoretic mobility in response to LPS stimulation was investigated in immortalized MK2/3-DKO bone-marrow macrophages reconstituted with MK2 or empty vector as negative control (vector). Inhibitors for $p38^{MAPK}$ (SB203580) or MK2 (Inh III) were co-applied during LPS treatment where indicated. (**e**) Endogenous RIPK1 was immunoprecipitated from control and short- (20 min) or long-term (90 min) LPS-stimulated, MK2-reconstituted DKO macrophages, in the presence and absence of additional MK2 (PF) and IKK (BMS) inhibitors as indicated. Co-precipitation of MK2 is evident, and this is enhanced by PF pretreatment and decreases on prolonged LPS stimulation. (**f**) *Yersinia* infection induces a time-dependent alteration of the RIPK1 electrophoretic mobility. J774A.1 macrophages were left untreated (ø), infected with Ye or the YopP-negative mutant Ye-Δ*yopP*, or treated with LPS. At the denoted times after onset of stimulation, cellular lysates were prepared and subjected to anti-RIPK1 immunoblotting with anti-actin as loading control. (**g**) MK2/3-DKO bone-marrow macrophages reconstituted with MK2 or empty control vector were treated with *Yersinia* and processed as in **d**. Unprocessed original scans of blots are shown in Supplementary Fig. 7. Results shown are representative of two (**a**–**c**), three (**d**–**f**) or four (**g**) independent experiments, respectively.

However, *Yersinia* impairs not only $p38^{MAPK}$ activation, but also that of IKKβ. Because the IKK complex may phosphorylate RIPK1 to inhibit its cytotoxic potential[11], we evaluated whether $p38^{MAPK}$/MK2 signalling affects RIPK1-related cell death when IKKβ activity is simultaneously silenced. This resembles more closely the action of YopP, which inhibits both pathways. Similar to its effect in TNF-mediated MEF cell death (Fig. 5a,b), BMS treatment sensitized macrophages to undergo death following Ye-Δ*yopP* infection (Fig. 6h). The death rate provoked by BMS and Ye-Δ*yopP* was significantly boosted in MK2-deficient cells, and in WT cells treated with SB or PF (Fig. 6h). Consistently, CASP8 processing was enhanced in MK2-deficient cells or following SB treatment (Fig. 6i). Thus, $p38^{MAPK}$/MK2 activation promotes macrophage survival following IKK pathway impairment. Nec-1s treatment provided substantial protection in all investigated conditions (Fig. 6h). Nec-1s reduced apoptosis in BMS-treated and Ye-Δ*yopP*-infected cells and also diminished cytotoxicity induced by the additional application of SB or PF. Comparable results were obtained for LPS-stimulated macrophages (Fig. 6j), where $p38^{MAPK}$/MK2 inhibitors also efficiently blocked RIPK1 phosphorylation (Supplementary Fig. 4k). Similarly, primary BMDMs generated from MK2-KO and MK2/3-DKO mice displayed significantly reduced cell viability when treated

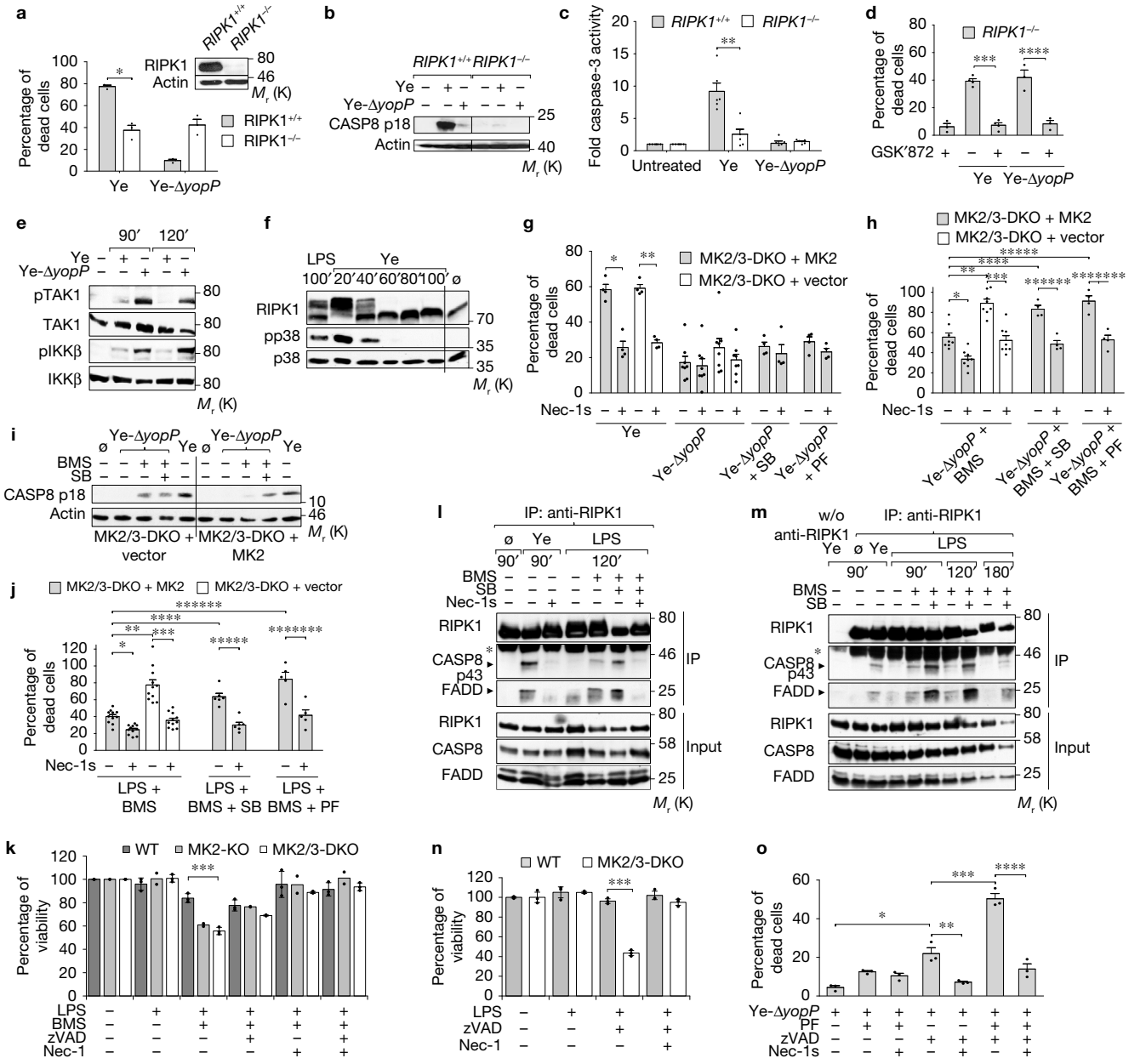

Figure 6 p38/MK2 signalling represses RIPK1-dependent death in infected macrophages. (**a**–**d**) *Yersinia* induces RIPK1-dependent apoptosis. (**a**) Death of WT (*RIPK*$^{+/+}$) and RIPK1-KO (*RIPK1*$^{-/-}$) macrophages infected with WT Ye or YopP-negative Ye-Δ*yopP* (6 h) (left) with immunoblot control (top right). (**b**) Appearance of active CASP8 p18 (3.5 h). (**c**) Caspase-3 activity in cell extracts (3 h). (**d**) Effect of the RIPK3 inhibitor GSK'872 on *RIPK1*$^{-/-}$ macrophage death (6 h). **a**,**c**,**d** show means ± s.e.m. (**a**: $^{*}P=0.001$, $n=3$; **c**: $^{**}P=0.0011$, $n=6$; **d**: $^{***}P<0.0001$, $n=4$; $^{****}P=0.0049$, $n=3$). (**e**) YopP impairs TAK1 and IKKβ phosphorylation in *RIPK1*$^{+/+}$ macrophages. (**f**) p38 inactivation correlates with downregulation of RIPK1 phosphorylation by YopP in J774A.1 macrophages. (**g**) Death of MK2-positive (MK2/3-DKO + MK2) or MK2-negative (MK2/3-DKO + vector) macrophages infected with Ye or Ye-Δ*yopP* in the presence of Nec-1s, p38 (SB) or MK2 (PF) inhibitors (5.5 h). (**h**–**j**) IKKβ and p38^{MAPK}/MK2 cooperatively inhibit RIPK1-dependent death. Death of macrophages stimulated with Ye-Δ*yopP* (**h**) or LPS (**j**) in the presence of Nec-1s, SB, PF or IKKβ inhibitor BMS (4–5 h), and CASP8 processing probed at 3.5 h of infection (**i**). **g**,**h**,**j** show means ± s.e.m. (**g**: $^{*}P=0.0004$, $^{**}P=0.0001$, $n=4$; **h**: $^{*}P=0.0009$, $^{**}P=0.0001$, $^{***}P=0.0001$, $n=8$; $^{****}P=0.0353$, $^{*****}P=0.0002$, $^{******}P=0.0006$, $^{*******}P=0.0015$, $n=4$; **j**: $^{*}P=0.0001$, $^{**}P=0.0001$, $^{***}P=0.0001$, $n=11$; $^{****}P=0.0025$, $^{*****}P=0.0001$, $n=6$; $^{******}P=0.0006$, $^{*******}P=0.0035$, $n=5$). (**k**) Viability of primary BMDMs from WT ($n=3$), MK2-KO ($n=2$) or MK2/3-DKO ($n=3$) mice treated as indicated (5 h); average percentage ± s.d. ($^{***}P=0.00069$). (**l**,**m**) Co-precipitation of CASP8 p43 and FADD with RIPK1 in MK2-rescued DKO macrophages (IP immunoprecipitation; the asterisk denotes the heavy chain of IP-IgG). Lysates were probed for input control. (**n**,**o**) MK2 inhibition promotes necroptosis. (**n**) Viability of primary WT or MK2/3-DKO BMDMs treated as indicated (5 h); average percentage ± s.d. ($n=3$ independent wells, $^{***}P=3.11\times10^{-5}$). (**o**) Death of J774A.1 macrophages treated as indicated (18 h); means ± s.e.m. ($n=3$, $^{*}P=0.0052$, $^{**}P=0.0085$, $^{***}P=0.0022$, $^{****}P=0.0007$). Samples in spliced panels (**b**,**f**,**i**) were obtained and processed simultaneously. Unprocessed blots are shown in Supplementary Fig. 7. **k** shows data from an experiment with BMDMs derived from the indicated numbers of mice; **n** is representative of two independent experiments. In all other panels, *n* represents the number of independent experiments. Statistical analysis by two-tailed unpaired *t*-test; statistical source data are provided in Supplementary Table 1 and reproducibility information is in the Methods.

with LPS/BMS compared with WT control cells (Fig. 6k). Death of the primary cells was efficiently suppressed by Nec-1, but only partially prevented by the pan-caspase inhibitor zVAD, probably reflecting the shift from RIPK1-dependent apoptosis to necroptosis following caspase inhibition. Thus, IKKβ inhibition and simultaneous $p38^{MAPK}$/MK2 pathway suppression trigger RIPK1-kinase activity-dependent apoptosis in response to bacterial infection and LPS treatment. Consistently, the interaction of RIPK1 with FADD and cleaved CASP8 p43 was substantially increased and stabilized when RIPK1 phosphorylation was inhibited by SB in LPS-stimulated and BMS-treated macrophages (Fig. 6m). This ripoptosome-like complex formation was sensitive to Nec-1s treatment (Fig. 6l). Thus, IKKβ and $p38^{MAPK}$/MK2 inhibition triggers assembly of a RIPK1-containing complex in infected macrophages that requires RIPK1-kinase activity for its pro-apoptotic action. These data together indicate that the concerted targeting of $p38^{MAPK}$/MK2 and IKKβ by YopP de-represses RIPK1 to provoke rapid apoptosis. Importantly, MK2 protected against LPS/TLR4- and *Yersinia*-triggered necroptosis[38] independent of IKK inhibition (Fig. 6n,o and Supplementary Fig. 5b). Thus, MK2 may prevent RIPK1-mediated cell death independent of IKK. An anti-apoptotic effect of MK2 on RIPK1 was furthermore seen in SM-induced macrophage apoptosis (Supplementary Fig. 5c,d).

DISCUSSION

Here, we describe RIPK1-dependent cell death control by the stress- and cytokine-activated $p38^{MAPK}$/MK2 pathway. MK2 phosphorylates RIPK1 and inhibition of $p38^{MAPK}$/MK2-mediated phosphorylation enhances RIPK1-kinase-dependent cytotoxicity. The physiological relevance of cytoprotective RIPK1 phosphorylation by MK2 is demonstrated by the ability of the *Y. enterocolitica* YopP protein to trigger apoptosis in infected macrophages by targeting TAK1, MAP2K members, and IKKβ (refs 35–37). YopP inhibition of anti-apoptotic signalling by IKKβ and $p38^{MAPK}$/MK2 unleashes RIPK1 cytotoxic activity, triggering RIPK1-kinase-dependent apoptosis.

RIPK1 is subjected to complex phosphorylation[39] including four to five autophosphorylation events and six to seven events possibly mediated by other kinases[13]. Five potential IKKα/IKKβ phosphorylation sites on hRIPK1 were deduced *in vitro* (Ser25, Ser166, Ser296, Ser331, Ser416; ref. 11). Of those, Ser330/Ser331 and Ser416 are IKK-dependently phosphorylated in cells[40]. Here, we identified Ser321 and Ser336 on mRIPK1 (Ser320 and Ser335 in hRIPK1) as MK2 phosphorylation sites. These are different from the IKK phosphorylation sites and, hence, could account for the detected bimodal regulation of RIPK1 by MK2 additive to that of IKKs. Phosphorylation of Ser321 by MK2 has recently been confirmed[41]. IKK phosphorylates only ubiquitylated RIPK1 in TNFR complex I (ref. 11). MK2 seems to mainly phosphorylate the cytoplasmic RIPK1 pool, independently of receptor recruitment, as non-TNFR-interacting RIPK1 mutants were also phosphorylated by MK2, MK2 was not recruited to TNFR and it interacted with a fraction of cytosolic RIPK1 already in non-stimulated cells. MK2 and IKK may thus not only target distinct sites, but also follow different spatio-temporal dynamics of RIPK1 phosphorylation, wherein IKK targets receptor-associated RIPK1 (such as in complex I), and MK2 phosphorylates RIPK1 in the cytoplasm. These phosphorylations do not seem mutually exclusive, as phosphorylation events attributed to MK2 (Ser321) and IKK (Ser332) (ref. 40) were detected on the same peptide (Supplementary Fig. 1d).

IKK phosphorylation is assumed to lock RIPK1 in an inactive conformation unable to autophosphorylate and execute cell death[11,42]. We find that inactivation of both RIPK1-phosphorylating kinases is required for effective release of its cytotoxic potential. RIPK1 autophosphorylation correlates with assembly and activation of death-inducing complexes[3,4,32] and, as expected from the increased RIPK1 autophosphorylation following $p38^{MAPK}$/MK2 inhibition, there was enhanced formation of a cytotoxic ripoptosome-like complex in LPS-stimulated macrophages (Fig. 6m). However, MK2 is not part of this death-promoting complex, as indicated by diminished co-immunoprecipitation of MK2 with RIPK1 under apoptosis-inducing conditions (Fig. 5e, BMS+PF+LPS 90′). Hence, a sequential scenario appears plausible (Supplementary Fig. 6): IKK inhibits activation of membrane-associated RIPK1, preventing cytosolic death-inducing complex seeding (checkpoint 1), and MK2 blocks cytotoxic signal amplification by inhibiting activation and integration of cytosolic RIPK1 into the cell death complex (checkpoint 2). However, the checkpoints can be uncoupled under certain conditions as lack of MK2 activity promoted LPS-dependent macrophage necroptosis without requiring IKK inhibition.

The MK2-dependent RIPK1 phosphosites could create a perfect binding site for 14-3-3 proteins[43–45]. As the major regulatory ubiquitylation site Lys376 and the CASP8 cleavage site Asp325 are in direct vicinity, 14-3-3 binding may interfere with these post-translational events by either shielding the CASP8 cleavage site or preventing ubiquitin ligase docking. A phosphorylation-defective RIPK1-S321A/S336A mutant showed stronger constitutive autophosphorylation and polyubiquitylation (Fig. 4g,f), suggesting that Ser321/336 phosphorylation could prevent polyubiquitylation. Ubiquitylation may stabilize RIPK1-containing cytotoxic complexes[33,46]. Whereas enhanced Ser166 phosphorylation of the S321A/336A mutant was consistent with the effects observed following MK2 inactivation, constitutive autophosphorylation associated with the S321D/S336D mutant was unexpected. It indicates that Ser166 phosphorylation and the cytoprotective effect are uncoupled by overexpressing RIPK1 with mutations in the seemingly sensitive interface located near the Ser321/Ser336 phosphosites. Thus, Ser166 phosphorylation does not always correlate with cell death and the MK2-dependent protection may operate downstream of Ser166 phosphorylation, indicating that this event is a marker for the MK2 effect only in cells expressing endogenous RIPK1 levels. Identification of specific RIPK1 substrates will be necessary to unravel the events downstream of RIPK1 activation in apoptosis/necroptosis.

The consequences of $p38^{MAPK}$/MK2-mediated RIPK1 phosphorylation remain to be investigated in disease models. MK2- and MK2/3-knockout mice exhibit defective LPS-induced TNF production and resistance against endotoxic shock[19,20]. Defective TNF biosynthesis may mask a protective role of MK2 in TNF- and RIPK1-mediated cytotoxicity. MK2-deficient mice display hypersensitivity and increased cellular damage against low TNF doses[47]. This is consistent with a suppressive function of MK2 on RIPK1-induced cell death and in agreement with Dondelinger *et al.*[48], showing

that MK2 inhibition sensitizes mice to RIPK1-dependent cytotoxic shock. As activation of the $p38^{MAPK}$/MK2 axis is downstream of pro-inflammatory RIPK1 signalling, feedback phosphorylation of RIPK1 by MK2 may suppress RIPK1-related cell death and support its pro-inflammatory activity in many cell stress conditions to optimize the immune response. Macrophage death during *Yersinia* infection is also host protective[49,50]. Thus, the cytoprotective phosphorylations of RIPK1 by MK2 and IKK, and also cytotoxicity due to their inhibition by YopP, are regulated processes activated within a controlled host immune response. MK2, IKK and RIPK1 therefore form a signalling triad linking inflammation and cell death, with decisive consequences on host immunity. □

METHODS

Methods, including statements of data availability and any associated accession codes and references, are available in the online version of this paper.

Note: Supplementary Information is available in the online version of the paper

ACKNOWLEDGEMENTS

We would like to acknowledge K. A. Fitzgerald, M. A. Kelliher, A. T. Ting and W. Brune for the gift of RIPK1-deficient cell lines, G. Tiegs and C. Wegscheid for providing the *Tnfr1*$^{-/-}$ mice, A. Pich for MS analysis, G. Evan, V. M. Dixit, J. Tschopp, and M. Treier for sharing expression vectors, A. Schambach for providing pLBID lentiviral vector, M. Windheim for discussion of results, K. Laaß for experimental support and T. Yakovleva for technical help. We thank A. Gossler for critical reading of the manuscript, J. C. Silva for help with phosphoproteomics, and I. Braren and the UKE HEXT Vector Facility for establishment of a lentiviral transduction system. This study was supported by grants from the Deutsche Forschungsgemeinschaft DFG to K.R. (Ru788/3-2 and Ru788/6-1) and M.G. (SFB566, TP B12).

AUTHOR CONTRIBUTIONS

M.B.M., J.G., A.K., M.G. and K.R. conceived the experiments and analysed the results. M.B.M., J.G., J.F., L.N., A.D., J.L., H.S., N.C. and N.R. performed the experiments. M.A. provided expertise and feedback. M.G. and K.R. secured funding. M.B.M., M.G. and K.R. wrote the manuscript.

COMPETING FINANCIAL INTERESTS

The authors declare no competing financial interests.

Published online at http://dx.doi.org/10.1038/ncb3614

1. Christofferson, D. E., Li, Y. & Yuan, J. Control of life-or-death decisions by RIP1 kinase. *Annu. Rev. Physiol.* **76,** 129–150 (2014).
2. Ofengeim, D. & Yuan, J. Regulation of RIP1 kinase signalling at the crossroads of inflammation and cell death. *Nat. Rev. Mol. Cell Biol.* **14,** 727–736 (2013).
3. Pasparakis, M. & Vandenabeele, P. Necroptosis and its role in inflammation. *Nature* **517,** 311–320 (2015).
4. Weinlich, R. & Green, D. R. The two faces of receptor interacting protein kinase-1. *Mol. Cell* **56,** 469–480 (2014).
5. Cusson-Hermance, N., Khurana, S., Lee, T. H., Fitzgerald, K. A. & Kelliher, M. A. Rip1 mediates the Trif-dependent toll-like receptor 3- and 4-induced NF-κB activation but does not contribute to interferon regulatory factor 3 activation. *J. Biol. Chem.* **280,** 36560–36566 (2005).
6. Meylan, E. *et al.* RIP1 is an essential mediator of Toll-like receptor 3-induced NF-κB activation. *Nat. Immunol.* **5,** 503–507 (2004).
7. Dannappel, M. *et al.* RIPK1 maintains epithelial homeostasis by inhibiting apoptosis and necroptosis. *Nature* **513,** 90–94 (2014).
8. Lalaoui, N. *et al.* Targeting p38 or MK2 enhances the anti-leukemic activity of Smac-mimetics. *Cancer Cell* **29,** 145–158 (2016).
9. Ea, C.-K., Deng, L., Xia, Z.-P., Pineda, G. & Chen, Z. J. Activation of IKK by TNFα requires site-specific ubiquitination of RIP1 and polyubiquitin binding by NEMO. *Mol. Cell* **22,** 245–257 (2006).
10. Li, H., Kobayashi, M., Blonska, M., You, Y. & Lin, X. Ubiquitination of RIP is required for tumor necrosis factor α-induced NF-κB activation. *J. Biol. Chem.* **281,** 13636–13643 (2006).
11. Dondelinger, Y. *et al.* NF-κB-independent role of IKKα/IKKβ in preventing RIPK1 kinase-dependent apoptotic and necroptotic cell death during TNF signaling. *Mol. Cell* **60,** 63–76 (2015).
12. Cho, Y. S. *et al.* Phosphorylation-driven assembly of the RIP1-RIP3 complex regulates programmed necrosis and virus-induced inflammation. *Cell* **137,** 1112–1123 (2009).
13. Degterev, A. *et al.* Identification of RIP1 kinase as a specific cellular target of necrostatins. *Nat. Chem. Biol.* **4,** 313–321 (2008).
14. Gaestel, M. MAPKAP kinases—MKs—two's company, three's a crowd. *Nat. Rev. Mol. Cell Biol.* **7,** 120–130 (2006).
15. Gaestel, M., Kotlyarov, A. & Kracht, M. Targeting innate immunity protein kinase signalling in inflammation. *Nat. Rev. Drug Discov.* **8,** 480–499 (2009).
16. Ronkina, N. *et al.* Stress induced gene expression: a direct role for MAPKAP kinases in transcriptional activation of immediate early genes. *Nucl. Acids Res.* **39,** 2503–2518 (2011).
17. Heidenreich, O. *et al.* MAPKAP kinase 2 phosphorylates serum response factor *in vitro* and *in vivo*. *J. Biol. Chem.* **274,** 14434–14443 (1999).
18. Tiedje, C. *et al.* The RNA-binding protein TTP is a global post-transcriptional regulator of feedback control in inflammation. *Nucl. Acids Res.* **44,** 7418–7440 (2016).
19. Kotlyarov, A. *et al.* MAPKAP kinase 2 is essential for LPS-induced TNF-α biosynthesis. *Nat. Cell Biol.* **1,** 94–97 (1999).
20. Ronkina, N. *et al.* The mitogen-activated protein kinase (MAPK)-activated protein kinases MK2 and MK3 cooperate in stimulation of tumor necrosis factor biosynthesis and stabilization of p38 MAPK. *Mol. Cell Biol.* **27,** 170–181 (2007).
21. Lehner, M. D. *et al.* Mitogen-activated protein kinase-activated protein kinase 2-deficient mice show increased susceptibility to *Listeria monocytogenes* infection. *J. Immunol.* **168,** 4667–4673 (2002).
22. Tiedje, C. *et al.* The p38/MK2-driven exchange between tristetraprolin and HuR regulates AU-rich element-dependent translation. *PLoS Genet.* **8,** e1002977 (2012).
23. Menon, M. B. *et al.* Endoplasmic reticulum-associated ubiquitin-conjugating enzyme Ube2j1 is a novel substrate of MK2 (MAPKAP kinase-2) involved in MK2-mediated TNFα production. *Biochem. J.* **456,** 163–172 (2013).
24. Tiedje, C. *et al.* p38MAPK/MK2-mediated phosphorylation of RBM7 regulates the human nuclear exosome targeting complex. *RNA* **21,** 262–278 (2015).
25. Lee, T. H., Shank, J., Cusson, N. & Kelliher, M. A. The kinase activity of Rip1 is not required for tumor necrosis factor-α-induced IκB kinase or p38 MAP kinase activation or for the ubiquitination of Rip1 by Traf2. *J. Biol. Chem.* **279,** 33185–33191 (2004).
26. Sun, X., Yin, J., Starovasnik, M. A., Fairbrother, W. J. & Dixit, V. M. Identification of a novel homotypic interaction motif required for the phosphorylation of receptor-interacting protein (RIP) by RIP3. *J. Biol. Chem.* **277,** 9505–9511 (2002).
27. Sanz, L., Sanchez, P., Lallena, M. J., Diaz-Meco, M. T. & Moscat, J. The interaction of p62 with RIP links the atypical PKCs to NF-κB activation. *EMBO J.* **18,** 3044–3053 (1999).
28. Feoktistova, M. *et al.* cIAPs block Ripoptosome formation, a RIP1/caspase-8 containing intracellular cell death complex differentially regulated by cFLIP isoforms. *Mol. Cell* **43,** 449–463 (2011).
29. Tenev, T. *et al.* The Ripoptosome, a signaling platform that assembles in response to genotoxic stress and loss of IAPs. *Mol. Cell* **43,** 432–448 (2011).
30. Schwermann, J. *et al.* MAPKAP kinase MK2 maintains self-renewal capacity of haematopoietic stem cells. *EMBO J.* **28,** 1392–1406 (2009).
31. Berger, S. B. *et al.* Cutting Edge: RIP1 kinase activity is dispensable for normal development but is a key regulator of inflammation in SHARPIN-deficient mice. *J. Immunol.* **192,** 5476–5480 (2014).
32. Newton, K. RIPK1 and RIPK3: critical regulators of inflammation and cell death. *Trends Cell Biol.* **25,** 347–353 (2015).
33. de Almagro, M. C., Goncharov, T., Newton, K. & Vucic, D. Cellular IAP proteins and LUBAC differentially regulate necrosome-associated RIP1 ubiquitination. *Cell Death Dis.* **6,** e1800 (2015).
34. Trosky, J. E., Liverman, A. D. B. & Orth, K. *Yersinia* outer proteins: Yops. *Cell. Microbiol.* **10,** 557–565 (2008).
35. Mukherjee, S. *et al.* *Yersinia* YopJ acetylates and inhibits kinase activation by blocking phosphorylation. *Science* **312,** 1211–1214 (2006).
36. Mittal, R., Peak-Chew, S.-Y. & McMahon, H. T. Acetylation of MEK2 and I κ B kinase (IKK) activation loop residues by YopJ inhibits signaling. *Proc. Natl Acad. Sci. USA* **103,** 18574–18579 (2006).
37. Paquette, N. *et al.* Serine/threonine acetylation of TGFβ-activated kinase (TAK1) by *Yersinia pestis* YopJ inhibits innate immune signaling. *Proc. Natl Acad. Sci. USA* **109,** 12710–12715 (2012).
38. He, S., Liang, Y., Shao, F. & Wang, X. Toll-like receptors activate programmed necrosis in macrophages through a receptor-interacting kinase-3-mediated pathway. *Proc. Natl Acad. Sci. USA* **108,** 20054–20059 (2011).
39. Dondelinger, Y., Vandenabeele, P. & Bertrand, M. J. M. Regulation of RIPK1's cell death function by phosphorylation. *Cell Cycle* **15,** 5–6 (2016).
40. Koppe, C. *et al.* IκB kinaseα/β control biliary homeostasis and hepatocarcinogenesis in mice by phosphorylating the cell-death mediator receptor-interacting protein kinase 1. *Hepatology* **64,** 1217–1231 (2016).
41. Jaco, I. *et al.* MK2 phosphorylates RIPK1 to prevent TNF-induced cell death. *Mol. Cell* **66,** 698–710.e5 (2017).
42. Dillon, C. P. & Balachandran, S. StIKKing it to a death kinase: IKKs prevent TNF-α-induced cell death by phosphorylating RIPK1. *Cytokine* **78,** 47–50 (2016).

43. Reinhardt, H. C. *et al*. p53-deficient cells rely on ATM- and ATR-mediated checkpoint signaling through the p38MAPK/MK2 pathway for survival after DNA damage. *Cancer Cell* **11,** 175–189 (2007).
44. Stoecklin, G. *et al*. MK2-induced tristetraprolin:14-3-3 complexes prevent stress granule association and ARE-mRNA decay. *EMBO J.* **23,** 1313–1324 (2004).
45. Blasius, M., Wagner, S. A., Choudhary, C., Bartek, J. & Jackson, S. P. A quantitative 14-3-3 interaction screen connects the nuclear exosome targeting complex to the DNA damage response. *Genes Dev.* **28,** 1977–1982 (2014).
46. Dondelinger, Y., Darding, M., Bertrand, M. J. M. & Walczak, H. Poly-ubiquitination in TNFR1-mediated necroptosis. *Cell. Mol. Life Sci.* **73,** 2165–2176 (2016).
47. Vandendriessche, B. *et al*. MAPK-activated protein kinase 2-deficiency causes hyperacute tumor necrosis factor-induced inflammatory shock. *BMC Physiol.* **14,** 5 (2014).
48. Dondelinger, Y. *et al*. MK2 phosphorylation of RIPK1 regulates TNF-mediated cell death. *Nat. Cell Biol.* **19,** 1237–1247 (2017).
49. Weng, D. *et al*. Caspase-8 and RIP kinases regulate bacteria-induced innate immune responses and cell death. *Proc. Natl Acad. Sci. USA* **111,** 7391–7396 (2014).
50. Philip, N. H. *et al*. Caspase-8 mediates caspase-1 processing and innate immune defense in response to bacterial blockade of NF-κB and MAPK signaling. *Proc. Natl Acad. Sci. USA* **111,** 7385–7390 (2014).

DOI: 10.1038/ncb3614

METHODS

Antibodies and reagents. Primary and secondary antibodies used in this study are listed in Supplementary Table 2. Reagents used for cell stimulations and treatments and their standard working concentrations were: lipopolysaccharide (*Escherichia coli* O55:B5) at 1 μg ml^{-1}, recombinant mouse TNF/human TNF (also known as TNFα) (Biomol) at 10–50 ng ml^{-1}, recombinant human TNF (Peprotech) at 20 ng ml^{-1}, FLAG-TNF (Enzo) at 1 μg ml^{-1}, anisomycin (Sigma) at 5–10 μg ml^{-1}, recombinant human IL-1α (Promocell) at 5 ng ml^{-1}, and birinapant Smac mimetics (Chemietek) at 5–10 μM. Where indicated, the cells were treated with specific inhibitors 1 h prior to stimulation. The inhibitors and the standard concentrations used were: pan-caspase inhibitor zVAD-fmk (zVAD; Bachem) at 20–25 μM; CASP3 inhibitor Ivachtin (Axon Medchem) at 10 μM; pan-IKK inhibitor TPCA-1 (TPCA; Tocris Bioscience) at 5 μM (ref. 39); IKKβ inhibitor BMS-345541 (BMS; Sigma) at 3–10 μM (ref. 51); JNK inhibitor SP600125 (Tocris Bioscience) at 10 μM; MEK1/2 inhibitor PD098059 (Tocris Bioscience) at 10 μM; MK2 Inhibitor III (Inh III; Calbiochem) at 20 μM, and MK2 inhibitor PF3644022 (Sigma-Aldrich) at 5–10 μM (ref. 52); p38 inhibitors SB203580 (SB; Tocris Bioscience) at 20 μM, VX-745 (Tocris Bioscience) at 5 μM, BIRB796 (Axon Medchem) at 1 μM; RIPK1 inhibitors Nec-1s (Focus Biomolecules) or Nec-1 (Enzo Life Sciences) at 50 μM (ref. 13); RIPK3 inhibitor GSK'872 (Calbiochem) at 2 μM (ref. 53); TAK1 inhibitors NP-009245 (NP; AnalytiCon Discovery), a derivative of the TAK1 kinase inhibitor 5Z-7-oxozeaenol, at 1 μM (ref. 54), and NG25 (MedChem Express) at 10 μM (ref. 55). Dimethylsulfoxide was included as solvent controls wherever necessary. All other reagents were obtained from Sigma.

Cells lines and culture conditions. SV40-T antigen immortalized WT, MK2 and MK2/3-deficient (DKO) mouse embryonic fibroblasts (MEFs) and retroviral rescued cells were reported previously[16,20]. 3T3-immortalized *Ripk1*$^{-/-}$ MEFs[56,57] from M. A. Kelliher (University of Massachusetts Medical School, Worcester, USA) were kindly provided by W. Brune (Heinrich-Pette-Institute, Hamburg, Germany)[58]. MEF cells and the human embryonic kidney (HEK) 293/HEK293T cell lines were cultured in DMEM cell growth medium containing 10% heat-inactivated fetal calf serum (FCS) and antibiotics. *Tnfr1*$^{-/-}$ mice and wild-type control mice were kindly provided by G. Tiegs and C. Wegscheid (Institute of Experimental Immunology and Hepatology, University Medical Center Hamburg-Eppendorf, Germany)[59]. MK2-KO (ref. 19) and MK2/3-DKO mice[20] were maintained at the animal facility of the Hannover Medical School. Primary bone-marrow macrophages were generated by flushing bone-marrow cells from the femurs of male and female mice at the age of 8 to 25 weeks as described previously and used after a total differentiation period of 8 days[60]. Handling of mice complied with all relevant ethical regulations and was approved by the ethics committees of Hannover Medical School and the Faculty of Medicine at the University of Hamburg. *Ripk1*$^{-/-}$ murine fetal liver macrophages and wild-type control macrophages immortalized with a J2 retrovirus were kindly provided by K. A. Fitzgerald (Division of Infectious Disease and Immunology, University of Massachusetts Medical School, Worcester, USA)[56,57]. Immortalized bone-marrow-derived macrophages established from wild-type mice or MK2/3-deficient mice (DKO), and DKO macrophage lines stably reconstituted with either MK2 (DKO + MK2) or empty vector control (DKO + vector) were reported previously[22]. The immortalized macrophage lines were cultured in DMEM with 10% heat-inactivated fetal calf serum and 1% non-essential amino acids. Murine J774A.1 macrophages were grown in RPMI 1640 medium supplemented with 10% heat-inactivated fetal calf serum and 5 mM L-glutamine[61]. All cells were incubated at 37 °C and with 5% CO_2 in a humidified atmosphere. The RIPK1-deficient Jurkat line was a gift from A. T. Ting (Mount Sinai School of Medicine, USA)[62] and was maintained in RPMI 1640 medium supplemented with 10% FCS, 1 mM pyruvate and antibiotics. Knockout cells and reconstituted cells were authenticated by western blotting as indicated. No further authentication was performed. The cell lines used were tested negative for mycoplasma contamination. Cells were observed and imaged using a Leica DM IL LED microscope and a Leica EC3 camera.

Phosphoproteomic analysis of MK2 substrates. MK2/3-deficient immortalized MEFs or bone-marrow-derived macrophages transduced with a MK2-expressing retrovirus or control cells were used for antibody-based phosphopeptide enrichment and LC–MS/MS analysis (Phosphoscan service, Cell Signaling Technology-CST). MEFs were stimulated for 30 min with anisomycin (10 μg ml^{-1}), lysates were digested by Glu-C protease, and the resulting peptides were immuno-affinity purified by a pPKD-motif-specific antibody. Macrophages were stimulated with LPS (1 μg ml^{-1}) for 30 min, lysates were subjected to Lys-C/trypsin digestion and phosphopeptide enrichment was performed using a cocktail of basophilic motif antibodies from CST consisting of pAKT-motif (no. 9614 and no. 10001), pAMPK-motif (no. 5759), pPKA-motif (no. 9624), pPKC-motif (no. 6967) and the pPKD-motif (no. 4381). The purified peptides were analysed at the CST facility by mass spectrometry (LC–MS/MS) in analytical duplicates and quantitatively compared using proprietary label-free quantification methods. The filtered quantitative phosphopeptide data together with protein/phosphosite assignment with accession numbers and additional details were provided by the company. Phosphopeptide information derived from the Phosphoscan relevant to the current study has been uploaded to Figshare and is available at https://doi.org/10.6084/m9.figshare.5272027.v1. These are not the raw data but are peptide enrichment data as provided by Cell Signaling Technology Phosphoscan.

Bacterial strains and infection. The *Y. enterocolitica* strains used in this study were the serotype O8 wild-type strain Ye, and its isogenic *yopP*-knockout mutant Ye-Δ*yopP*[61]. Prior to infection, overnight bacterial cultures grown at 27 °C were diluted 1:10 in fresh Luria–Bertani broth and grown for another 1.5 h at 37 °C. Shift of the growth temperature to 37 °C initializes activation of the *Yersinia* type-III secretion machinery for efficient translocation of Yops into the host cell following cellular contact. Cells were usually infected at a ratio of 20 bacteria per cell. For incubation times longer than 90 min, bacteria were routinely killed by addition of gentamicin (50 μg ml^{-1}) after 90 min of infection to prevent bacterial overgrowth.

Plasmids, cloning and mutagenesis. The mouse RIPK1 coding region was PCR-amplified from total MEF (mouse embryonic fibroblast) cDNA and cloned into the pENTR-D-TOPO directional cloning vector (Invitrogen) following the manufacturer's protocol. The C-terminal truncations 1–588 and 1–500 were generated similarly using alternative reverse primers. All primers applied for cloning and mutagenesis of RIPK1 are listed in Supplementary Table 2. Site-directed mutagenesis was performed using the QuikChange mutagenesis kit (Stratagene). RIPK1-RHIM mutant (^{528}IQIG/AAAA^{531}) was generated by PCR amplification with reverse mutagenesis primer and *Ripk1*-fwd primer in two-step PCR, followed by Dpn I treatment, digestion with KpnI/EcoRI and ligation into similarly digested pENTR-RIPK1. Destination expression vectors with GFP, GST, Myc and FLAG tags for mammalian/bacterial expression were generated by LR recombination reactions (Invitrogen). FLAG-tagged mRIPK1 and mutants were PCR-amplified from the pDEST-FLAG vector and were subcloned into the AgeI/XhoI sites in the pLBID-GFP-P2A-puro vector to generate lentiviral expression vectors. Myc-mRIPK1, FLAG-hRIPK1 and hRIPK3 vectors were gifts from G. Evan (UCSF Cancer Center, USA), V. M. Dixit (Genentech, USA) and J. Tschopp (Lausanne, Switzerland), respectively. The HA-ubiquitin expression vector was kindly provided by M. Treier (European Molecular Biology Laboratory, Heidelberg, Germany). All other plasmids used were described previously[23,30].

Lentiviral vectors and transduction. pLBID vector (GFP, puromycin resistance, kind gift from A. Schambach, Hannover, Germany) encoding wild-type/mutant FLAG-mRIPK1 or empty vector was packaged using the three-vector packaging system (Virapower, Thermo Fischer Scientific) in HEK293T cells, following the standard procedure. Untagged mRIPK1-WT and mutants were cloned into the NheI/XmaI sites of the pSicoR-Ef1a-mCherry-2A-Puro lentiviral vector (derived from Addgene plasmid no. 31848 pSicoR-Ef1a-mCh-Puro-GFPi)[63], replacing the mCherry-CDS, and the resulting vectors were packaged by co-transfection with psPAX2 (Addgene plasmid no. 12260)/pMD2.G (Addgene plasmid no. 12259) packaging plasmids at a ratio of 3:2:1. Viral supernatants were collected 48 h post transfection, filtered through 45 μm filters, and were then used for transducing MEFs (overnight incubation with viral particles and 8 μg ml^{-1} Polybrene) or spinoculating RIPK1-deficient Jurkat cells (1 million cells with 1 ml virus spun at 800*g* for 90 min at 32 °C in the presence of 8 μg ml^{-1} Polybrene). Cells were washed and medium changed after overnight virus treatment and selected in the presence of 1–4 μg ml^{-1} puromycin, until non-transduced cells are completely dead. Transduction in pLBID-transduced cells was monitored by flow cytometry (>97% GFP-positive) using an Accuri-C6 cytometer (BD Biosciences).

Intracellular staining and flow cytometric analysis of RIPK1 expression. MEF cells suspended in PBS were fixed with 3× volume PFA (4%) at room temperature for 30 min, washed, resuspended in PBS, and absolute methanol was added to 90% concentration with constant mixing. The methanol permeabilization was continued for 30 min on ice. After 2× PBS wash cells were resuspended in 4% BSA-PBS, blocked on ice for 30 min and stained with anti-RIPK1 antibodies (BD Biosciences no. 610459, 1:100 diluted in 1%BSA-PBS) at room temperature for 60 min. After 1× PBS wash, samples were resuspended in secondary antibody dilution (anti mouse Alexa Fluor-488—1:700 diluted in 1% BSA-PBS) and incubated for an additional 30 min before PBS wash and analysis on a BD-Accuri-C6 flow cytometer.

Transient transfection. For transfection of HEK293/HEK293T cells, cells were seeded 24 h earlier to reach approximately 80–90% confluence. Transfection was performed using polyethylenimine (PEI; Sigma-Aldrich) or ProFection reagent (Promega). PEI-transfection was performed under antibiotic-free conditions and medium was changed 12–16 h post addition of complexes. Transfected cells were

analysed between 20 and 36 h post transfection. To inhibit the spontaneous phosphorylation of overexpressed RIPK1, cells were treated with inhibitors for the last 3 h before lysis.

Knockdown of RIPK1 in J774A.1 macrophages. shRNA targeting a C-terminal region of mouse RIPK1 (primers listed in Supplementary Table 2) was cloned into the lentiviral vector LeGO-G-puromycin[64] using HpaI and XhoI restriction sites. A vector with a scrambled shRNA sequence insert was used as control. Pseudotyped lentiviral supernatants containing LeGO-G-puromycin shRNA were generated in HEK293 cells by co-transfecting expression plasmids for HIV Rev, Gag/Pol and VSV-G Env using ProFection reagent (Promega). The supernatants were harvested 24, 48 and 72 h post transfection and used for transduction of J774A.1 macrophages. The viral particles were centrifuged on the cells (1 h, 800*g*, 37 °C) in the presence of 8 μg ml^{-1} Polybrene (Sigma-Aldrich). The cell culture medium was replaced after 16 h and transduced cells were selected for 3 days by puromycin treatment. The RIPK1 protein levels in the transduced cells were determined by western immunoblotting.

Cell lysis and immunoblotting. Cells were solubilized with RIPA lysis buffer containing 150 mM NaCl, 1% NP-40, 0.5% DOC, 0.1% SDS, 50 mM Tris (pH 8.0), 1 mM EDTA, 1 mM EGTA, 20 mM β-glycerophosphate, 0.4 mM phenylmethylsulfonyl fluoride, 1 mM NaF, 1 mM Na_3VO_4, plus additional phosphatase and protease inhibitors (Roche Diagnostics) and subjected to several freeze–thaw cycles on dry ice–ethanol bath. The lysates were cleared by centrifugation, separated by SDS–PAGE, and transferred to polyvinylidene difluoride (PVDF) membrane. In other cases, cells were directly lysed by boiling in 2× SDS–PAGE loading buffer and analysed by immunoblotting as described previously[65]. Immunoreactive bands were visualized using appropriate secondary antibodies and enhanced chemiluminescence detection reagents. Uncropped western blots for key experimental results are shown in Supplementary Fig. 7.

Subcellular fractionation. Separation of membrane and cytosolic fractions was performed essentially as described previously[66]. Cells were scraped out in homogenization buffer (250 mM sucrose, 20 mM Tris-HCl (pH 7.5), 1 mM $MgCl_2$, 1 mM $MnCl_2$, 10 mM β-glycerophosphate supplemented with protease and phosphatase inhibitor cocktails—Bimake) and disrupted by passing through a 25 G needle attached to a 1 ml syringe. Nuclei and unbroken cells were removed by low-speed centrifugation (1,000*g* for 10 min at 4 °C) and homogenates were ultracentrifuged at 100,000*g* for 1 h at 4 °C in a TLA 100.4 rotor (Beckman-Coulter). The pellets (P100) containing cellular membranes resuspended in 2× SDS–PAGE loading buffer and the supernatants (cytosol, S100) diluted 1:1 with the loading buffer were analysed by SDS–PAGE and immunoblotting.

Immunoprecipitation and GST-pulldowns. For Myc-MK2 immunoprecipitation, cells were lysed in immunoprecipitation buffer (50 mM HEPES, 150 mM NaCl, 1.5 mM $MgCl_2$, 2 mM KCl, 10% glycerol, 1 mM EDTA, 1 mM EGTA, 1% Triton X-100, plus phosphatase and protease inhibitors (Roche Diagnostics)) and subjected to two freeze–thaw cycles on dry ice–ethanol bath. The lysates were then incubated with anti-Myc (no. 2276; Cell Signaling Technology) antibodies. The immune complexes were collected with protein A/G-agarose (Santa Cruz Biotechnology), washed four times with lysis buffer, treated with sample buffer and subjected to SDS–PAGE and immunoblotting. For the precipitation of endogenous RIPK1 from macrophages, the cells were lysed in a buffer containing 10 mM Tris pH 8.0, 1% NP-40, 10% glycerol, 150 mM NaCl, 1 mM EDTA, plus phosphatase and protease inhibitors (Roche Diagnostics). RIPK1 was precipitated by using monoclonal anti-RIPK1 antibody (no. 610459; BD Biosciences) and the ImmunoCruz IP/WB Optima C System (sc-485040; Santa Cruz Biotechnology). To detect interaction with MK2, the anti-RIPK1 antibody was crosslinked to protein A/G-agarose beads before immunoprecipitation by applying BS3 according to the manufacturer's instructions (Thermo Fisher Scientific). For kinase assays, RIPK1 was immunoprecipitated from lysed cells and subjected to *in vitro* kinase assays with [γ-^{32}P]ATP as recommended previously[67]. GST-pulldowns[23] and FLAG-IPs[24] were performed essentially as described previously. During GST-pulldown to enrich the ripoptosome-like complexes, transfected cells were treated with the CASP3 inhibitor Ivachtin to reduce massive RIPK1-induced death. For analysing the RIPK1 ubiquitylation, RIPK1-reconstituted MEFs were transfected with HA-ubiquitin expression vector and treated as indicated 1 d later. Cells were subsequently lysed by boiling in 1% SDS and lysates were subjected to RIPK1 immunoprecipitation after dilution of the samples to 0.1% SDS in RIPA buffer as described previously[68].

Enrichment of the TNFR-associated complex for monitoring RIPK1 ubiquitylation. MEFs grown in 10 cm plates were stimulated with 1 μg ml^{-1} FLAG-hTNF (no. ALX-522-008-C050, Enzo Life Sciences) for 5 min at 37 °C. Control plates were shifted to ice 30 min before stimulation. Plates were washed 2× with ice-cold PBS and lysed in 500 μl lysis buffer (30 mM Tris-HCl pH 7.7, 120 mM NaCl, 2 mM KCl, 2 mM EDTA, 5% glycerol, 1% Triton X-100, 1× phosphatase inhibitor cocktail A (no. B15001, Bimake) and Protease inhibitor tablet (no. 04693124001, Roche)) on ice for 40 min. Scraped out lysates were cleared by centrifuging at maximum speed for 30 min at 4 °C. The supernatants were immunoprecipitated by overnight incubation with FLAG-M2 beads. The beads were washed twice with PBS + 1% Triton X-100 followed by two washes with PBS + 0.5% Triton X-100. The beads were boiled in 2× SDS loading dye and separated on 10% SDS–PAGE gels together with input controls.

Recombinant protein expression and purification. RIPK1-ΔC (1–500aa) was expressed from the pDEST-15 expression vector as a GST-fusion protein and purified from *Escherichia coli* BL21 cells using standard protocols. Glutathione–Sepharose (Amersham Biosciences) bead-bound wild-type and mutant GST-RIPK1-ΔC proteins were directly used for MK2-kinase assays using radioactive [γ-^{33}P]ATP as described previously[65].

Analysis of cytotoxicity, viability and caspase-3 activation. The rates of cell death were measured in duplicate or triplicate in a 96-well format by using Sytox Green Nucleic Acid Stain (Invitrogen). The cell impermeable dye was added to the cells 30 min before measurement at a final concentration of 0.5 μM. The intensity of Sytox Green in dead cells was then determined in a fluorescence plate reader (TriStar LB 942, Berthold Technologies) as a function of time[69]. The maximum Sytox Green intensity per well was calculated by adding Triton X-100 to each well at a final concentration of 0.5% and Sytox Green intensities were measured after 1 h (corresponding to 100% cell death). Results are expressed as percentages of cell death per well in relation to the background signal in non-induced cells and the maximal cell death rate according to the formula: percentage of cell death = [(induced cell death − background signal of non-induced cells)/(maximal cell death − background signal)] × 100 (ref. 69). Wherever indicated, WST-1 assay (Roche) was used to measure cell viability following the manufacturer's protocol. In experiments involving Nec-1, the medium was changed before the addition of diluted WST-1, to avoid interference.

The activity of caspase-3 as a marker of apoptosis was assessed using the fluorogenic substrate Ac-DEVD-AMC (Asp-Glu-Val-Asp cleavage) as described previously[69]. Briefly, cell extracts were prepared with caspase lysis buffer (1% NP-40, 10 mM Tris-HCl pH 7.4, 10 mM NaCl, 3 mM $MgCl_2$, 1 mM phenylmethylsulfonyl fluoride, 0.3 mM aprotinin, 1 mM leupeptin and 1 mM oxidized glutathione) and equal fractions thereof were diluted in caspase reaction buffer (10 mM HEPES-NaOH pH 7.4, 220 mM mannitol, 68 mM sucrose, 2 mM $MgCl_2$, 2 mM NaCl, 2.5 mM H_2KPO_4, 0.5 mM EGTA, 0.5 mM sodium pyruvate, 0.5 mM L-glutamine and 10 mM dithiothreitol) containing the caspase substrate Ac-DEVD-AMC (A1086, Sigma-Aldrich) at a final concentration of 50 μM. Reactions were performed at 37 °C for 1 h. The release of free AMC was measured every 2 min by determining fluorescence at 360 nm (excitation) and 460 nm (emission) in a multimode microplate reader (Infinite M200, Tecan). Values were calculated as fold differences in caspase-3 activity compared with non-stimulated cells (=1).

Statistics and reproducibility. Results of quantitative assays are expressed as means ± s.e.m./s.d. from *n* numbers of experiments or triplicate samples as indicated in the figure legends. Statistical analysis was performed using two-tailed unpaired *t*-test using GraphPad Prism or MS-Excel and *P* values are presented in the figure legends. A *P* value of <0.05 was considered statistically significant. Experimental repeats of shown representative results are indicated in the figure legends except for Fig. 6: Fig. 6b,e,f,l,n represents one out of two, and Fig. 6i,m one out of three independent experiments. Experiments shown in Fig. 2e and Supplementary Fig. 4d were performed once. All other representative experiments were successfully conducted at least twice. Shown viability data are representative of two (Fig. 6n) or three (Fig. 4b,c) independent experiments. Statistical source data and results of independent viability repeat experiments are provided in Supplementary Table 1. No statistical method was used to predetermine sample size and experiments were not randomized.

Data availability. Statistical source data for the quantitative results for Figs 4b,c,e and 6a,c,d,g,h,j,k,n,o and Supplementary Figs 3a,b,e,f,h, 4a,e,g–l and 5a–c are provided as Supplementary Table 1. Phosphopeptide information are not the raw data but are peptide enrichment data as provided by the Cell Signaling Technology Phosphoscan service and phosphopeptide data have been deposited at Figshare: https://doi.org/10.6084/m9.figshare.5272027.v1. All other data supporting the findings of this study are available from the corresponding authors on reasonable request.

DOI: 10.1038/ncb3614

51. Burke, J. R. *et al.* BMS-345541 is a highly selective inhibitor of I κ B kinase that binds at an allosteric site of the enzyme and blocks NF-κB-dependent transcription in mice. *J. Biol. Chem.* **278,** 1450–1456 (2003).
52. Mourey, R. J. *et al.* A benzothiophene inhibitor of mitogen-activated protein kinase-activated protein kinase 2 inhibits tumor necrosis factor α production and has oral anti-inflammatory efficacy in acute and chronic models of inflammation. *J. Pharmacol. Exp. Ther.* **333,** 797–807 (2010).
53. Kaiser, W. J. *et al.* Toll-like receptor 3-mediated necrosis via TRIF, RIP3, and MLKL. *J. Biol. Chem.* **288,** 31268–31279 (2013).
54. Vanlangenakker, N. *et al.* cIAP1 and TAK1 protect cells from TNF-induced necrosis by preventing RIP1/RIP3-dependent reactive oxygen species production. *Cell Death Differ.* **18,** 656–665 (2011).
55. Tan, L. *et al.* Discovery of type II inhibitors of TGFβ-activated kinase 1 (TAK1) and mitogen-activated protein kinase kinase kinase kinase 2 (MAP4K2). *J. Med. Chem.* **58,** 183–196 (2015).
56. Kelliher, M. A. *et al.* The death domain kinase RIP mediates the TNF-induced NF-κB signal. *Immunity* **8,** 297–303 (1998).
57. Kang, S. *et al.* Caspase-8 scaffolding function and MLKL regulate NLRP3 inflammasome activation downstream of TLR3. *Nat. Commun.* **6,** 7515 (2015).
58. Mack, C., Sickmann, A., Lembo, D. & Brune, W. Inhibition of proinflammatory and innate immune signaling pathways by a cytomegalovirus RIP1-interacting protein. *Proc. Natl Acad. Sci. USA* **105,** 3094–3099 (2008).
59. Rothe, J. *et al.* Mice lacking the tumour necrosis factor receptor 1 are resistant to TNF-mediated toxicity but highly susceptible to infection by *Listeria monocytogenes*. *Nature* **364,** 798–802 (1993).
60. Novikova, L. *et al.* Cell death triggered by *Yersinia enterocolitica* identifies processing of the proinflammatory signal adapter MyD88 as a general event in the execution of apoptosis. *J. Immunol.* **192,** 1209–1219 (2014).
61. Ruckdeschel, K. *et al. Yersinia* outer protein P of *Yersinia enterocolitica* simultaneously blocks the nuclear factor-κ B pathway and exploits lipopolysaccharide signaling to trigger apoptosis in macrophages. *J. Immunol.* **166,** 1823–1831 (2001).
62. Ting, A. T., Pimentel-Muiños, F. X. & Seed, B. RIP mediates tumor necrosis factor receptor 1 activation of NF-κB but not Fas/APO-1-initiated apoptosis. *EMBO J.* **15,** 6189–6196 (1996).
63. Salomonis, N. *et al.* Alternative splicing regulates mouse embryonic stem cell pluripotency and differentiation. *Proc. Natl Acad. Sci. USA* **107,** 10514–10519 (2010).
64. Weber, K., Bartsch, U., Stocking, C. & Fehse, B. A multicolor panel of novel lentiviral 'gene ontology' (LeGO) vectors for functional gene analysis. *Mol. Ther.* **16,** 698–706 (2008).
65. Menon, M. B. *et al.* p38 MAP kinase and MAPKAP kinases MK2/3 cooperatively phosphorylate epithelial keratins. *J. Biol. Chem.* **285,** 33242–33251 (2010).
66. Micheau, O. & Tschopp, J. Induction of TNF receptor I-mediated apoptosis via two sequential signaling complexes. *Cell* **114,** 181–190 (2003).
67. Degterev, A., Zhou, W., Maki, J. L. & Yuan, J. Assays for necroptosis and activity of RIP kinases. *Meth. Enzymol.* **545,** 1–33 (2014).
68. Moquin, D. M., McQuade, T. & Chan, F. K.-M. CYLD deubiquitinates RIP1 in the TNFα-induced necrosome to facilitate kinase activation and programmed necrosis. *PLoS ONE* **8,** e76841 (2013).
69. Vanden Berghe, T. *et al.* Determination of apoptotic and necrotic cell death *in vitro* and *in vivo*. *Methods* **61,** 117–129 (2013).

nature cell biology

DOI: 10.1038/ncb3614

In the format provided by the authors and unedited.

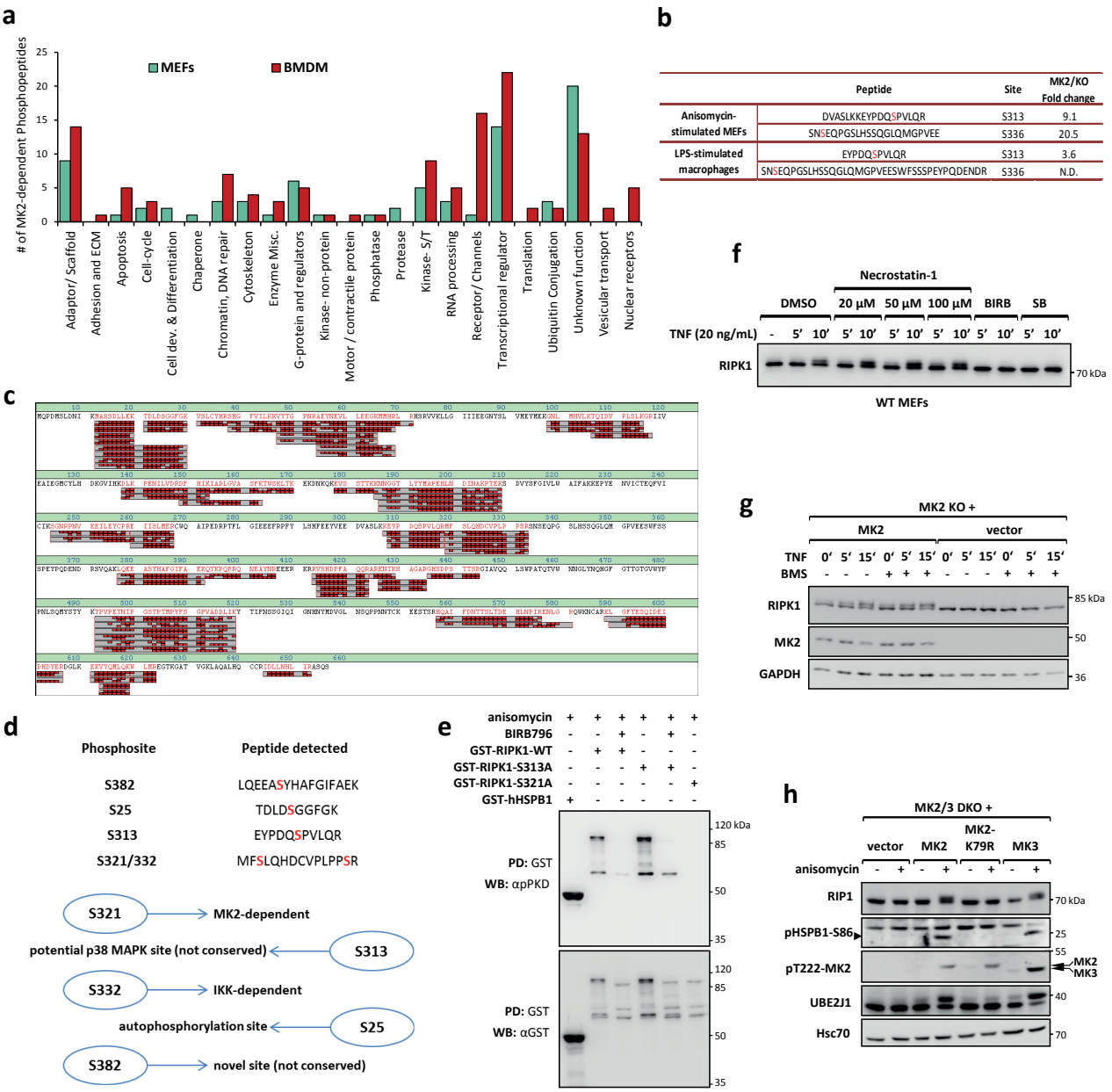

Supplementary Figure 1 Identification and characterisation of phosphorylation sites on RIPK1. **a.** Classification of phospho-peptides identified in anisomycin-stimulated MEFs and LPS-stimulated macrophages (BMDM), based on the gene-ontology class of the target proteins. **b.** Peptides detected in Phosphoscan analysis and fold changes dependent on the presence of MK2 (N.D: peptide not detected in KO samples). **c & d.** Mass-spectrometric analysis of GST-mRIPK1 purified from anisomycin-stimulated HEK293T cells. Total coverage (1c) and phospho-sites identified (1d), listed with additional available information on the respective sites based on literature and database searches. **e.** S313 is not required for p38/MK2-mediated phosphorylation of mRIPK1. HEK293T cells were transfected and subjected to GST-pull down and immunoblotting analysis as in Fig. 1d & 2d. Neither the mobility shift nor the phospho-PKD substrate motif antibody signals depend on the integrity of the S313 residue. **f.** The RIPK1 inhibitor Nec-1 does not inhibit the TNF- induced shift of murine RIPK1 even at concentration as high as 100 μM, while the shift is abrogated by two independent p38 MAPK inhibitors (BIRB796, 1 μM and SB202190, 5 μM). **g.** IKKβ inhibitor BMS345541 does not inhibit the TNF-induced MK2-dependent band-shift of RIPK1. **h.** Both MAPKAP kinases, MK2 and MK3 can mediate stress induced RIPK1 phosphorylation. MK2/3 DKO MEF cells were reconstituted with MK2, catalytic dead-MK2 (K79R), MK3 expression vector or an empty vector control. The cells were stimulated with anisomycin and subjected to immunoblot analysis to monitor the electrophoretic mobility shift of RIPK1. An antibody against MK2-T222 was used to detect activating phosphorylations of MK2 and MK3, Hsc70 is shown as loading control. The phosphorylation of bonafide substrates of MK2/3, HSPB1 (S86 phosphorylation) and UBE2j1 (band-shift), is shown as positive control. Results shown are representative of 2 (Suppl. Fig. 1e, 1h) and 3 (Suppl. Fig. 1f, 1g) independent experiments, respectively.

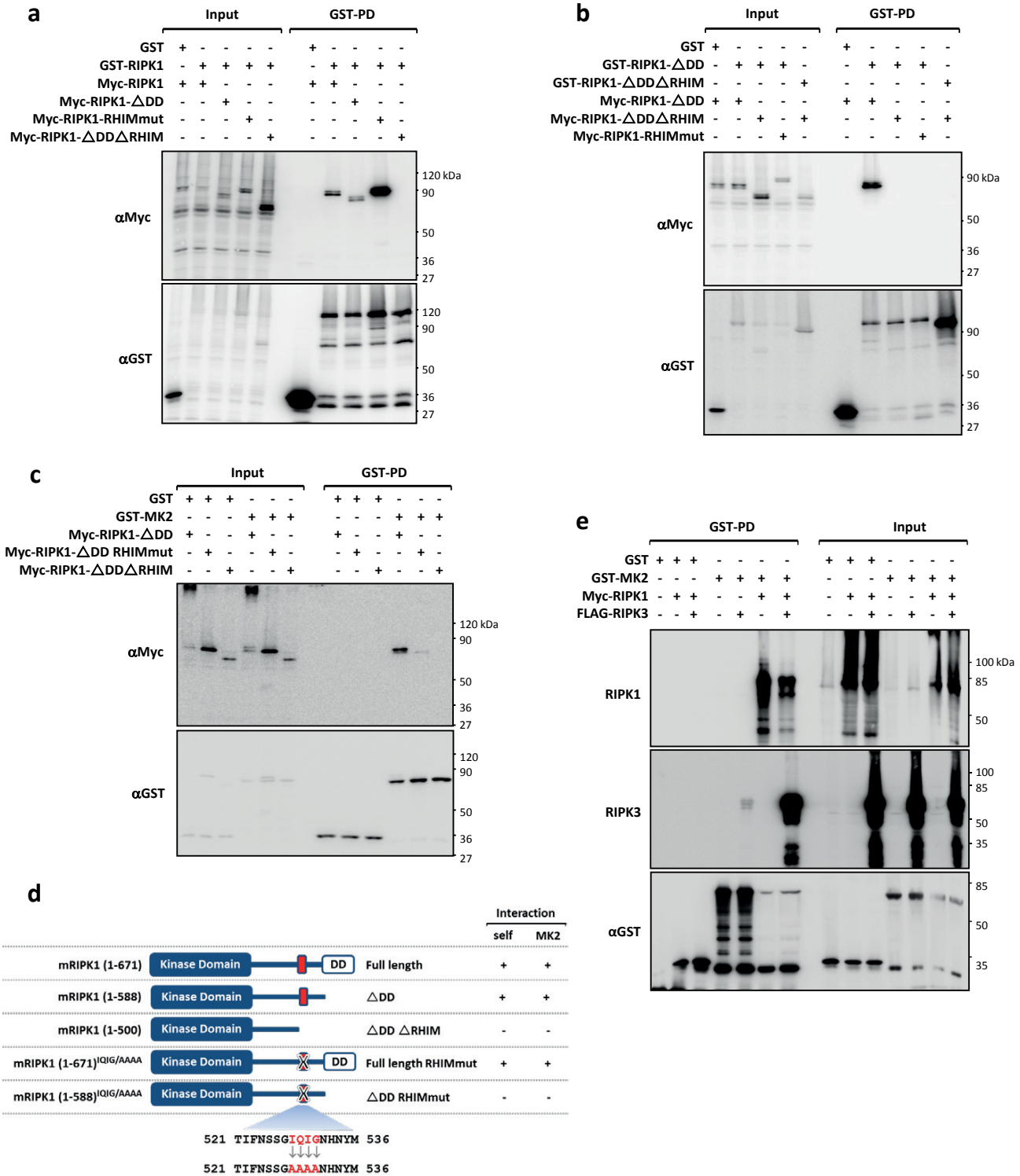

Supplementary Figure 2 MK2-RIPK1 interaction requires RIPK1-dimerisation and is independent of RIPK3. **a, b & c.** Indicated RIPK1 expression vectors (a, b) and MK2 vectors (c) were co-transfected in HEK 293T cells and RIPK1 self-association (a, b) and RIPK1-MK2 interaction were probed by using GST-pull down experiments. **d.** Schematic presentation of the RIPK1 mutants used in the study and summary of the findings indicating the capability of the different mutants to self-associate as well as to interact with MK2. Self-association or dimerization capacity seems to be a prerequisite for interaction with MK2. **e.** Recruitment of RIPK1 to MK2 does not depend on RIPK3, but MK2/RIPK1/RIPK3 can form a ternary complex. HEK293T cells were transfected with expression constructs for GST-MK2, Myc-RIPK1, FLAG-RIPK3 and control empty vector controls. 24 h post transfection, cell lysates were subjected to GST-pull down and the pull downs together with input controls were probed by western blotting. While Myc-RIPK1 is strongly and specifically enriched by GST-MK2, FLAG-RIPK3 enrichment is significant only when co-expressed with Myc-RIPK1, suggesting that RIPK1 bridges the MK2-RIPK3 interaction. Results shown in Suppl. Fig. 2a, 2b, 2c, 2e are representative of 2 independent experiments.

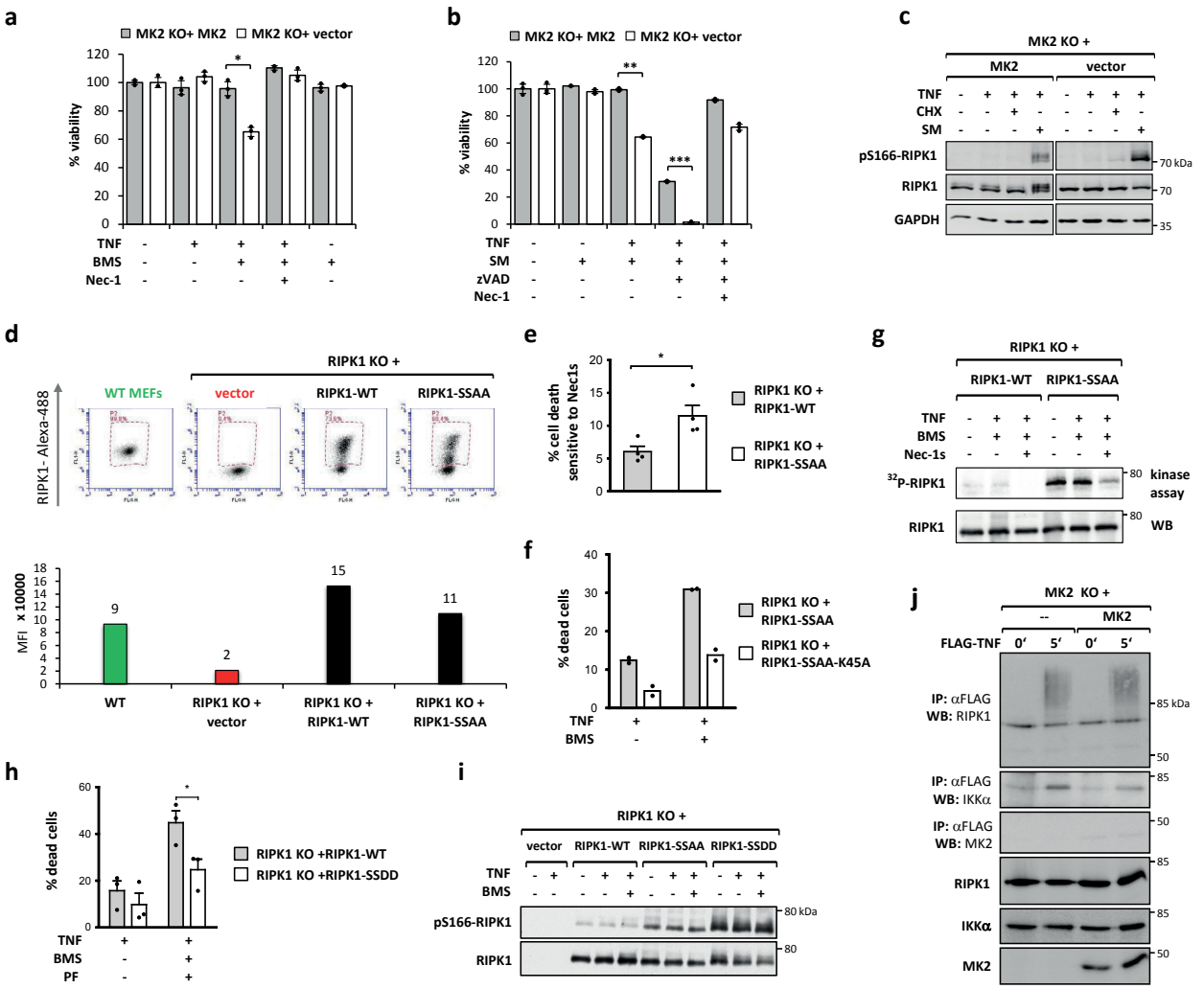

Supplementary Figure 3 MK2 suppresses RIPK1-dependent cell death and RIPK1 activity, but not receptor associated ubiquitination. **a & b.** MK2 KO MEFs transduced with MK2 or empty vector control were treated as indicated for 5 h and cell viability was assessed by WST-1-assay. Average values are plotted ± SD (*p=0.00303; **p=8.2x10^{-6}, ***p=3.9x10^{-7} n=3 independent wells). **c.** Cells were treated with 15 µg/ml cycloheximide (CHX) or 5 µM SM for 1h, followed by 2 h with 20 ng/ml TNF. Consistent with death assay data in panel 3b, immunoblot analysis of the lysates shows strong autophosphorylation of RIPK1 in response to TNF+SM treatment in MK2-deficient cells. The samples in the spliced panel were obtained and processed simultaneously. **d.** Flow cytometric analysis of RIPK1 expression in WT and RIPK1-KO-MEFs reconstituted with the indicated RIPK1 expression vectors or empty vector controls (top panel). The lower panel shows the median fluorescent intensity of RIPK1 staining in the positive-gated population. RIPK1-WT reconstituted cells show higher RIPK1 expression than WT MEFs and RIPK1-SSAA rescued cells. **e.** Percentages of necrostatin-sensitive RIPK1-dependent death from the data presented in Fig. 4e were quantified and plotted as mean ± SEM (n=4,*p=0.0227). **f.** RIPK1-SSAA mutation was combined with the K45A mutation and death assays were performed as in Fig. 4e. A representative experiment performed in duplicate is shown. **g.** RIPK1-WT- or RIPK1-SSAA-reconstituted RIPK1-KO-MEFs were treated as in Fig. 4f and immunoprecipitated RIPK1 was subjected to autophosphorylation in *in vitro*-kinase assay. RIPK1-westernblot is shown as IP-control. **h.** RIPK1 KO MEFs reconstituted with RIPK1-WT or RIPK1-S321D / S336D (RIPK1-SSDD) mutant were treated as indicated for 21 h and cell death was assessed as in Fig. 4e. Quantitative results are expressed as means ± SEM from n=3 independent experiments (*p=0.0417). **i.** MK2 KO MEFs transduced with MK2 expression vector or empty vector control were stimulated with 1 µg/ml FLAG-tagged TNF and the TNF-receptor complex was immunoprecipitated using αFLAG-M2 affinity beads. The immunoprecipitates and input lysates were probed with the indicated antibodies. Statistical analysis was performed using two-tailed unpaired t-test. Viability and cell death data of Suppl. Fig. 3a, 3b, 3f are representative of two (Suppl. Fig. 3b) or three (Suppl. Fig. 3a, 3f) independent experiments. Statistical source data and results of independent repeat experiments are provided in Supplementary Table 1. Shown immunoblot results are representative of 2 (Suppl. Fig. 3c, 3d, 3g, 3j) and 3 (Suppl. Fig. 3i) independent experiments, respectively.

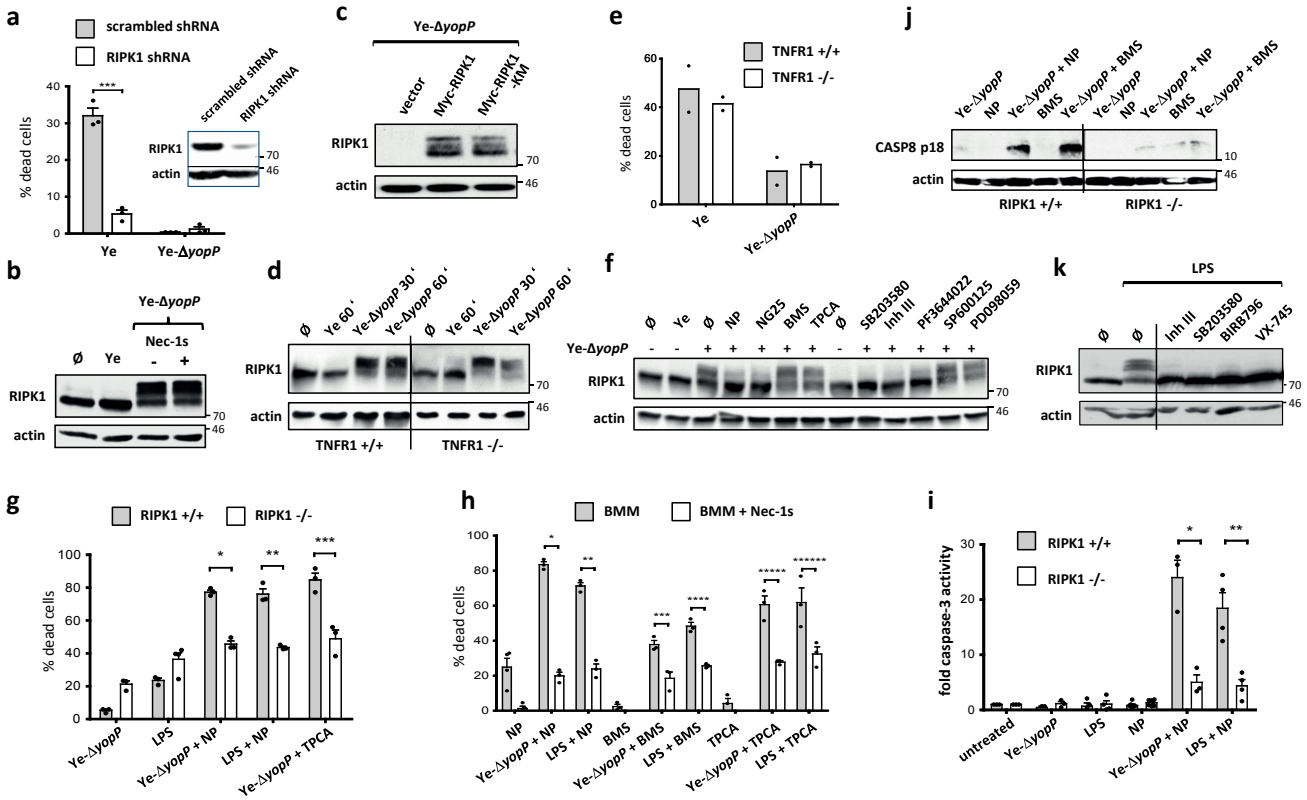

Supplementary Figure 4 *Yersinia*-induced apoptosis in macrophages: dissecting involvement of IKK, TAK1, p38/MK2 inhibition by YopP in RIPK1-dependent cytotoxicity. **a.** J774A.1 macrophages treated with lentiviral RIPK1 shRNA or scrambled control shRNA were infected with wild type *Y. enterocolitica* Ye, or YopP-negative Ye-Δ*yopP*. Dead cells were quantified after 5 h. Results are expressed as means ± SEM from n=3 independent experiments (***p=0.0003). RIPK1 protein levels were analyzed by immunoblotting and equal loading of the gels was controlled by determining the actin levels. **b & c.** RIPK1 phosphorylation occurs independent of RIPK1 activity. J774A.1 macrophages were infected with yersiniae in presence of the RIPK1 inhibitor Nec-1s where indicated (4b). In 4c, J774A.1 macrophages were transfected with Myc-tagged wild type RIPK1 or kinase-inactive K45A-RIPK1 mutant (KM) before infection. Empty pcDNA3 vector was used as control (vector). RIPK1 electrophoretic mobility was analyzed by immunoblotting in cell lysates prepared after 90 (4b), or 35 min of stimulation (4c) using anti-RIPK1 (4b) or anti-myc antibodies (4c). **d & e** Primary bone-marrow derived macrophages (BMDM) from WT (+/+) or TNFR1-KO (-/-) mice were infected with WT (Ye) or YopP-negative *Yersinia* (Ye-Δ*yopP*) and the mobility shift of RIPK1 was monitored by immunoblotting (4d). Cell death was quantified after 6.5 h and results are expressed as means from two independent experiments (4e). **f.** Inhibitors of TAK1, p38, and MK2 suppress RIPK1 phosphorylation induced by *Yersinia*. Immortalized RIPK1 +/+ fetal liver mouse macrophages were infected with YopP-negative Ye-Δ*yopP* in presence of inhibitors for TAK1 (NP, NG25), IKKβ (BMS), IKK (TPCA), p38 (SB203580), MK2 (Inh III, PF3644022), JNK (SP600125), or MEK1/ERK (PD098059). The phosphorylation of RIPK1 was analyzed by immunoblotting in cell lysates prepared after 75 min of infection. **g & h.** Infected macrophages treated with specific inhibitors of TAK1 or IKK undergo RIPK1-mediated cell death. RIPK1 +/+ and -/- immortalized fetal liver macrophages (4g) or immortalized BMDM (4h) were stimulated with Ye-Δ*yopP* or LPS in presence of inhibitors for TAK1 (NP), IKK (TPCA), IKKβ (BMS), and Nec-1s as indicated. Cell death was quantified after 5 h (4g) or 4 h (4h). **i & j.** NP and BMS trigger RIPK1-dependent apoptosis. Caspase-3 activation was monitored by analyzing DEVD-AMC cleavage in cell lysates prepared after 3 h of infection (4i). The generation of the active caspase-8 p18 (CASP8 p18) was assessed after 3.5 h of infection (4j). Results in 4g, 4h, 4i are expressed as means ± SEM from independent experiments (4g: *p=0.0002, **p=0.0007, ***p=0.0063, n=3; 4h: *p<0.0001, **p=0.0002, ***p=0.0108, ****p=0.0006, *****p=0.0028, ******p=0.0341, n=3; 4i: *p=0.005, n=3; **p=0.0036, n=4). **k.** J774A.1 macrophages were treated with LPS in presence of inhibitors for p38 (SB203580, BIRB796, VX-745) or MK2 (Inh III). RIPK1 phosphorylation was analyzed in cell lysates prepared after 90 minutes. The samples in the spliced panel of Fig. 4k were obtained and processed simultaneously. Statistical analysis was performed using two-tailed unpaired t-test and statistical source data are provided as Supplementary Table 1. Results shown are representative of 2 (Suppl. Fig. 4j), 3 (Suppl. Fig. 4c, 4f, 4k), or 4 (Suppl. Fig. 4b) independent experiments. The experiment of Suppl. Fig. 4d was performed once.

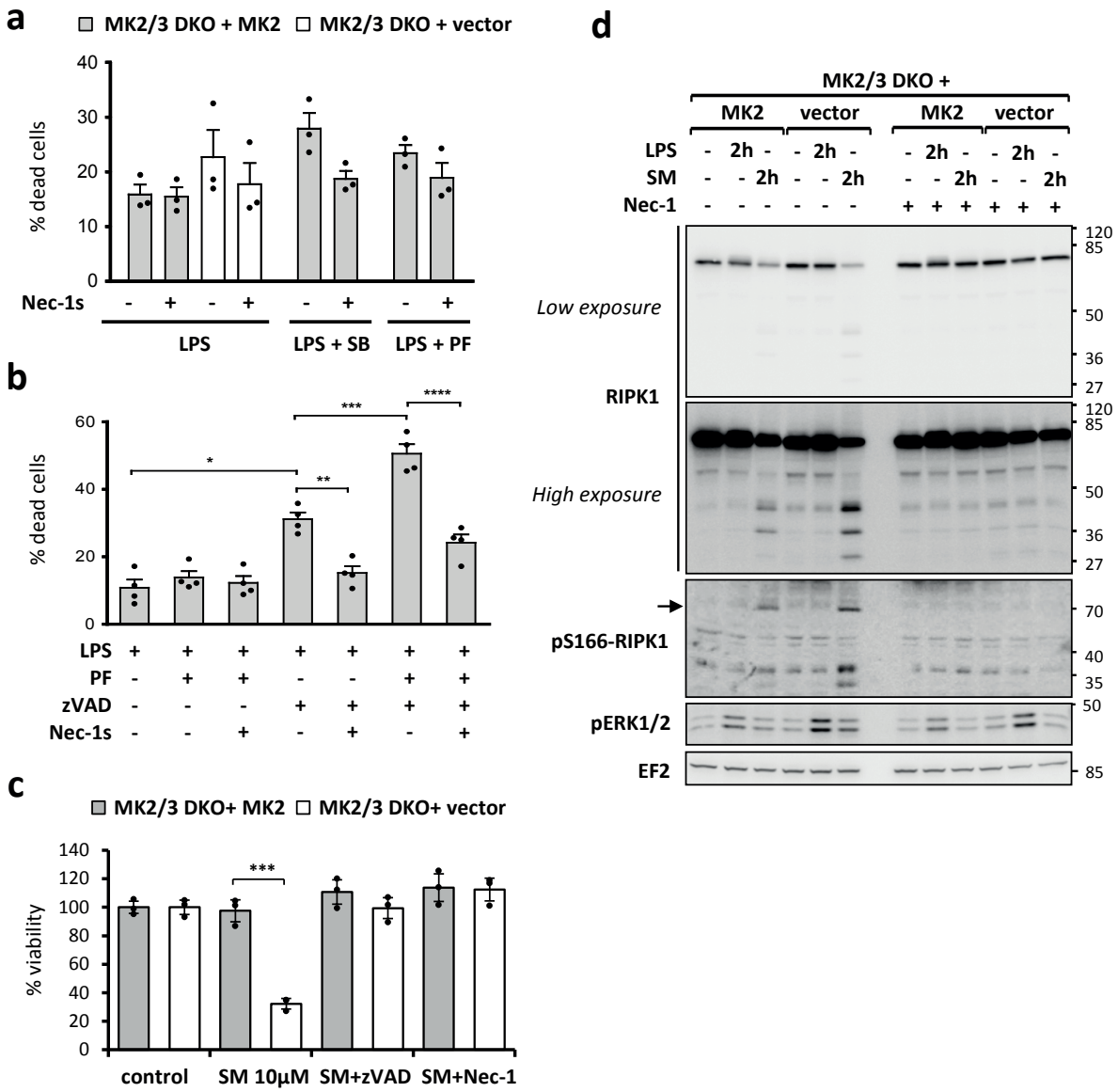

Supplementary Figure 5 Suppressive role of MK2 in LPS-dependent macrophage necroptosis as well as in SM-induced autocrine TNF-dependent apoptosis. **a.** $p38^{MAPK}$/MK2 inhibition alone has no major impact on cell viability in LPS-treated macrophages. MK2/3 DKO + MK2 or MK2/3 DKO + vector macrophages were stimulated with LPS in presence of Nec-1s, the p38 inhibitor SB or the MK2 inhibitor PF where indicated. Cell death was quantified after 4 h using Sytox Green Nucleic Acid Stain. Results are expressed as means ± SEM from n=3 independent experiments. **b.** MK2 inhibition promotes LPS-induced necroptosis of macrophages. J774A.1 macrophages were stimulated with LPS in presence of Nec-1s, the MK2 inhibitor PF and zVAD where indicated. Cell death was quantified after 14 h. Results are expressed as means ± SEM from n=4 independent experiments (*p = 0.0006, **p=0.0012, ***p=0.0013, ****p=0.0004). **c & d.** MK2 inhibition triggers SM-induced apotosis of macrophages Immortalized BMDMs of the indicated genotypes were treated with 10 µM Smac mimetics (SM) with or without 1 h pretreatment with the caspase-inhibitor zVAD or the RIPK1 inhibitor Necrostatin-1 (Nec-1). After 7 h, cell viability was assessed by WST-1 assay in n=3 independent wells (means ± SD, ***p=0.0209) (in c). Immortalized macrophages as indicated in panel 5c were treated with LPS or SM with or without 1 h pretreatment with Nec-1 for the shown time points. Cell lysates were probed with the indicated antibodies (in d). The cleavage of RIPK1 in the course of apoptosis is reduced in MK2-positive cells and prevented by RIPK1 inhibition. EF2 is shown as loading control and MAPK activation (pERK1/2) for monitoring stimulation. Statistical analysis was performed using two-tailed unpaired t-test. The viability experiment of Suppl. Fig. 5c is representative of three independent experiments. Statistical source data and results of independent repeat experiments are provided in Supplementary Table 1. The immunoblot result of Suppl. Fig. 5d is representative of 2 independent experiments.

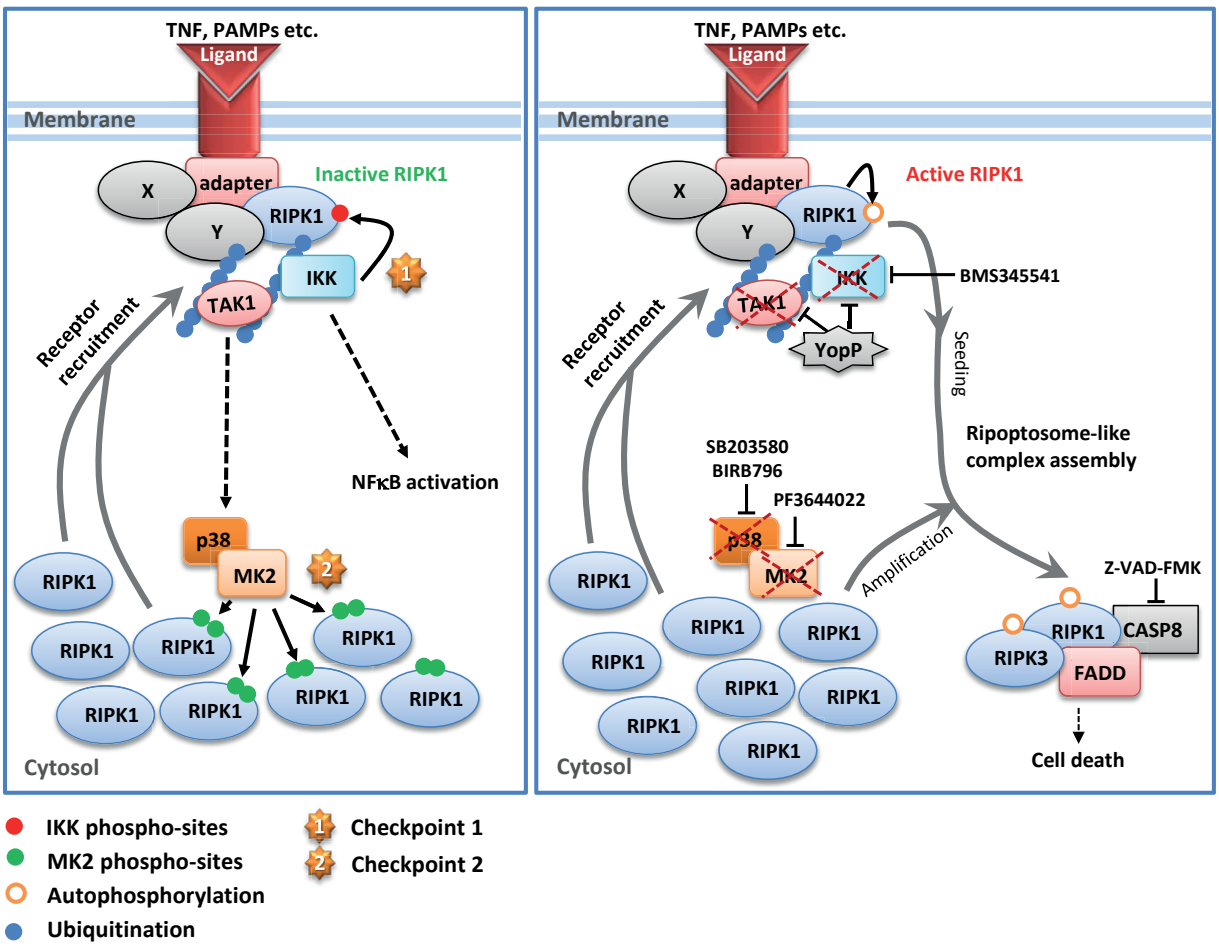

Supplementary Figure 6 Additive roles of the IKK- and p38^{MAPK}/MK2-dependent checkpoints in the suppression of cytotoxic RIPK1 signaling. Ligand binding induces recruitment of RIPK1 to the stimulated receptor and RIPK1 ubiquitination. The subsequent induction of TAK1 triggers downstream p38/MK2 activation, whereas the parallel recruitment of the IKK complex to poly-ubiquitinated RIPK1 mediates pro-survival NFκB activation and phosphorylation of receptor-associated RIPK1 (probably at murine S332 and human S331). MK2 activation downstream to TAK1-p38 signaling induces phosphorylation of the majority of cytosolic RIPK1 at S321/S336, which could further be recruited to the receptor complexes. These synergistic phosphorylation events by MK2 (cytosol, checkpoint 2) and IKK (receptor, checkpoint 1) keep RIPK1 activity and cytotoxicity under stringent control (left panel). When intermediate domain phosphorylation of RIPK1 is inhibited by YopP (inactivating TAK1 and IKK), or by pharmacological inhibition of p38/MK2 and IKK, RIPK1 undergoes activation and autophosphorylation. While activated RIPK1 dissociated from the receptor complex could seed for a cytosolic ripoptosome-like complex, non-phosphorylated RIPK1 in the cytosol could amplify the signal by enhancing cross autophosphorylation (in trans), which may subsequently promote the formation of fully functional RIPK1-containing complexes that elicit a strong pro-cytotoxic response (right panel).

Supplementary Fig. 7a

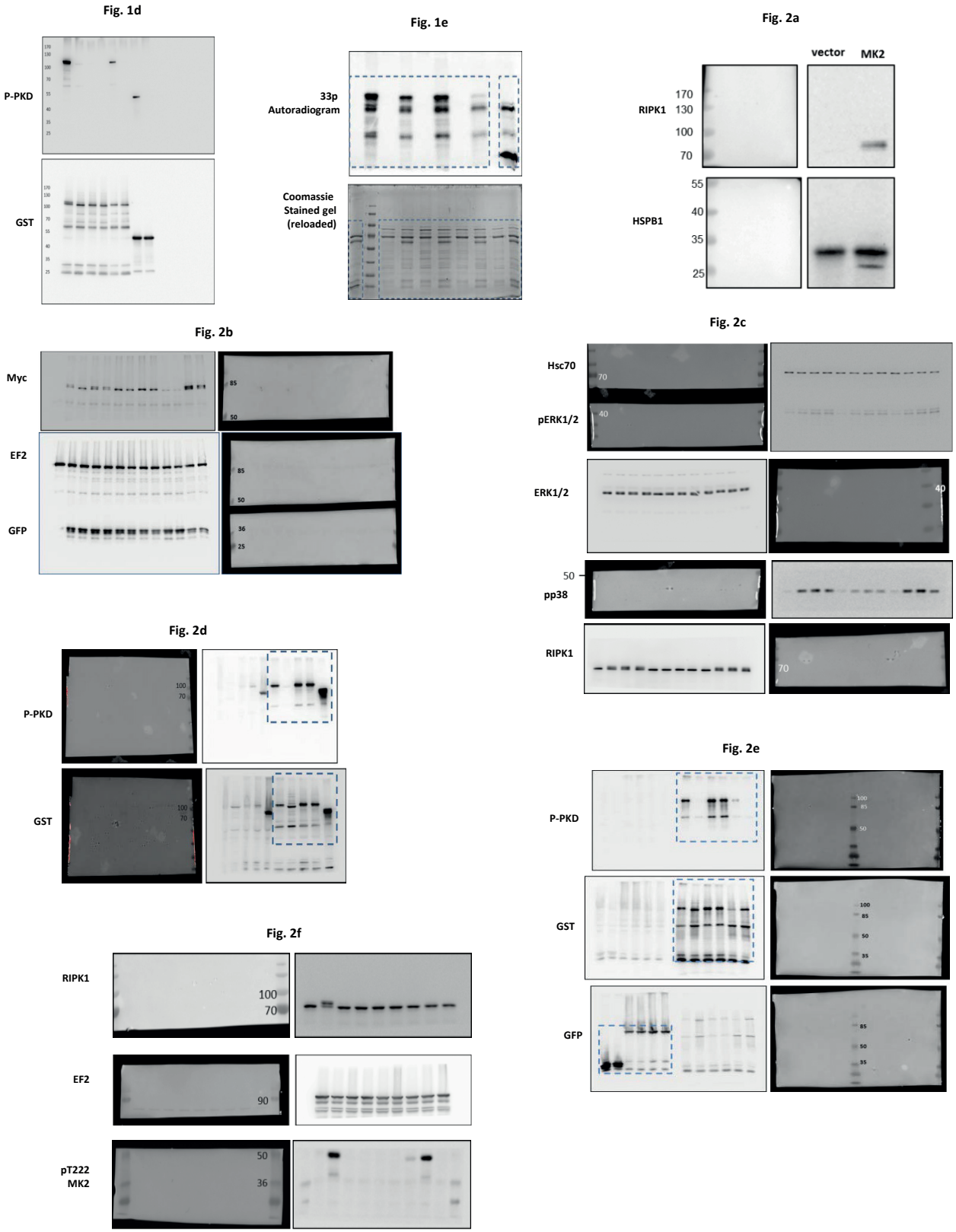

Supplementary Figure 7 Uncropped blots of crucial experiments presented in the manuscript. **a-e.** Uncropped and marker-aligned blots from key experiments are shown in Fig. 1 to Fig. 6.

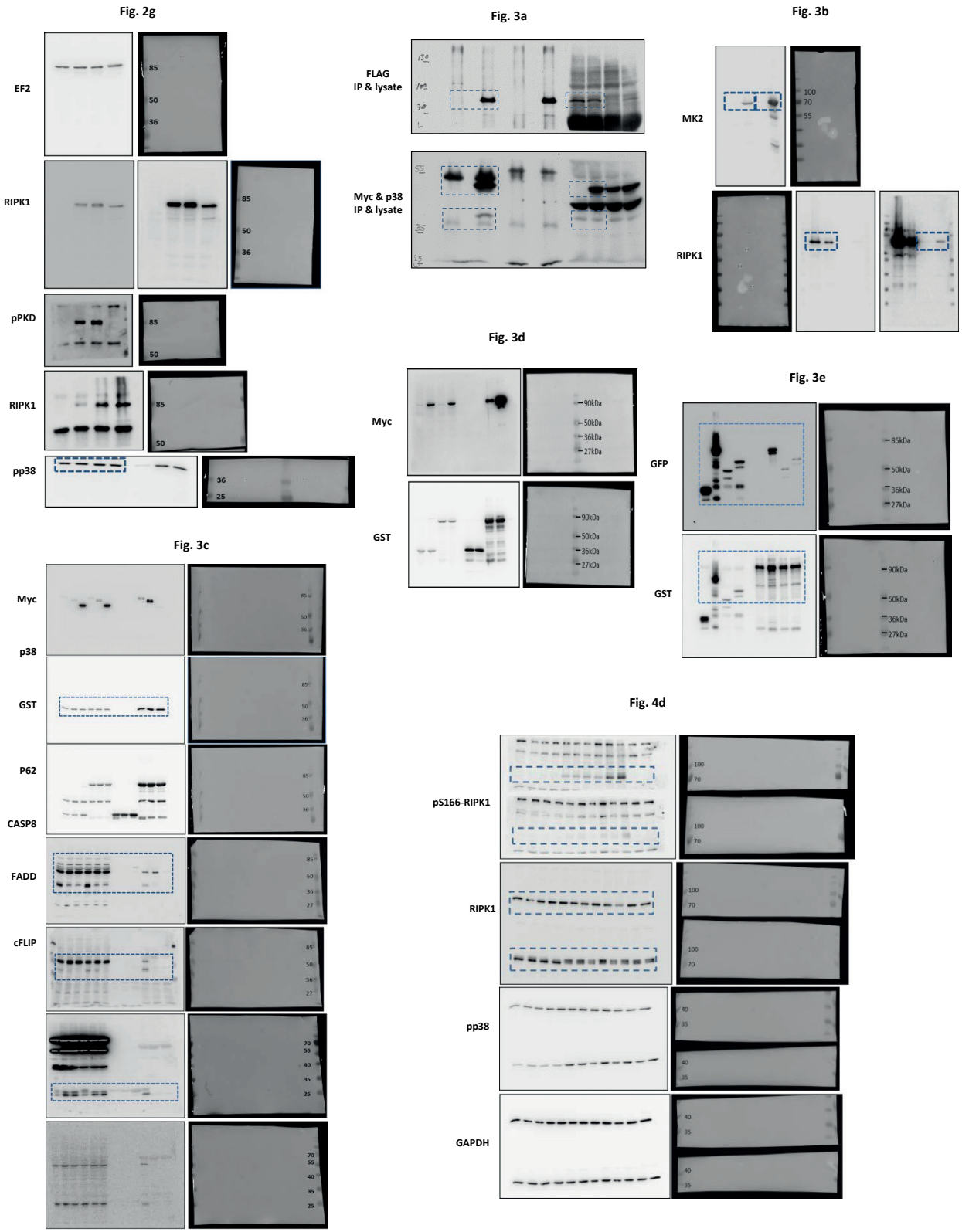

Supplementary Figure 7 Continued

Fig. 4f

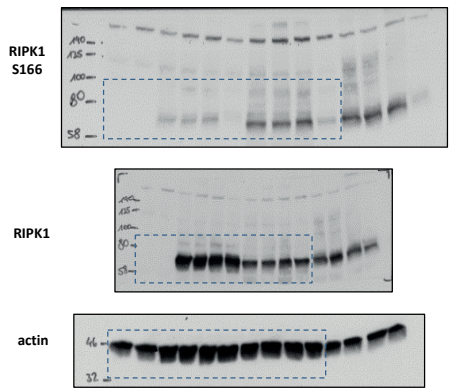

Fig. 4g

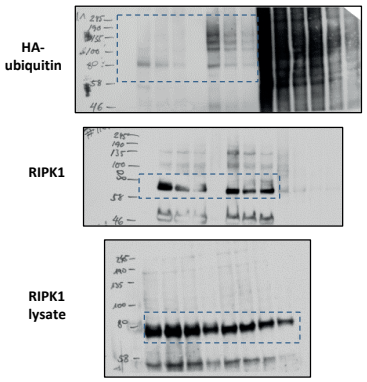

Fig. 5a

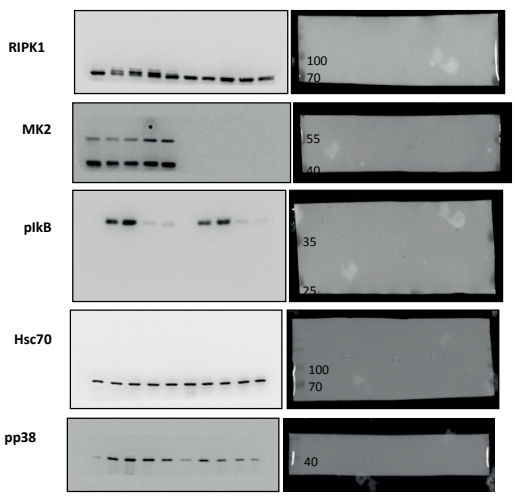

Fig. 5b

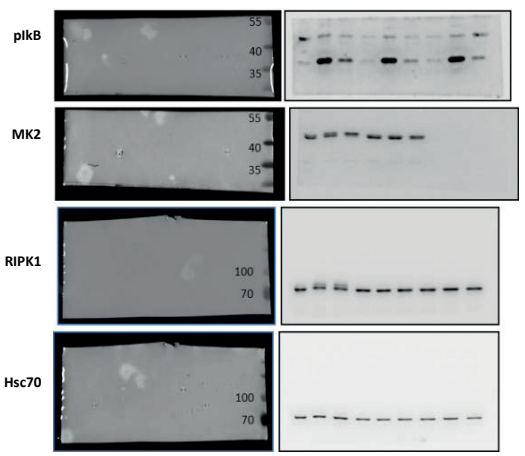

Fig. 5c

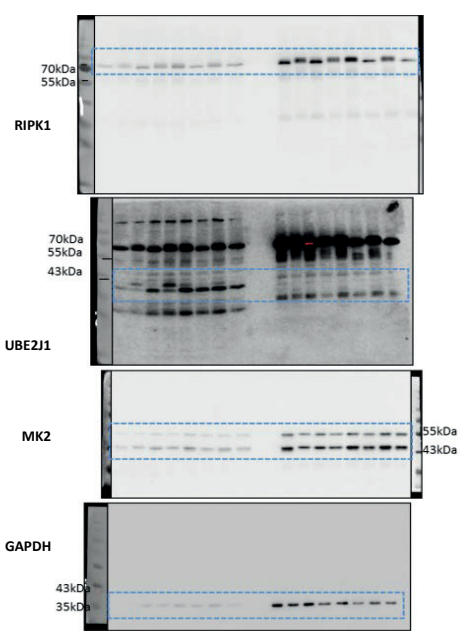

Fig. 5d

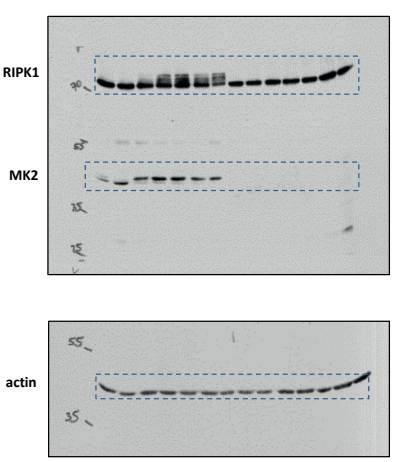

Fig. 5e

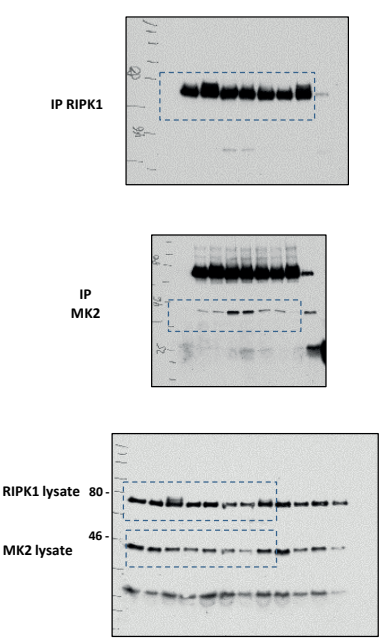

Supplementary Figure 7 Continued

Fig. 5f

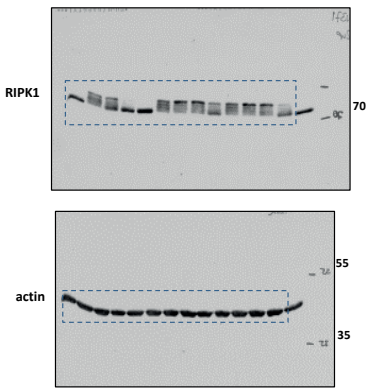

Fig. 5g

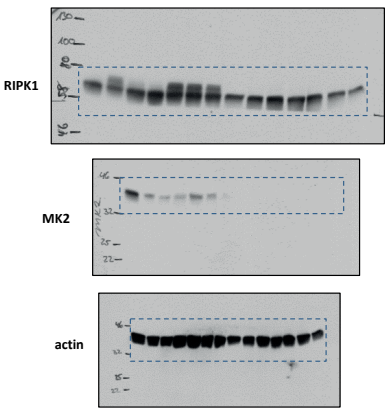

Fig. 6b

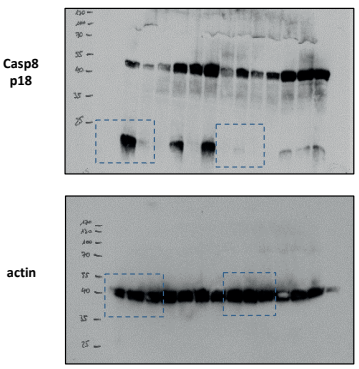

Fig. 6e

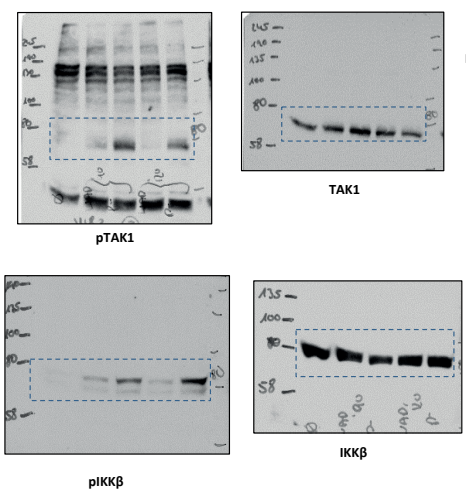

Fig. 6f

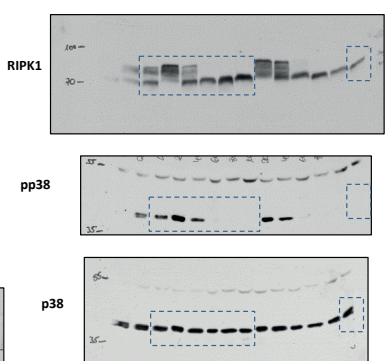

Fig. 6i

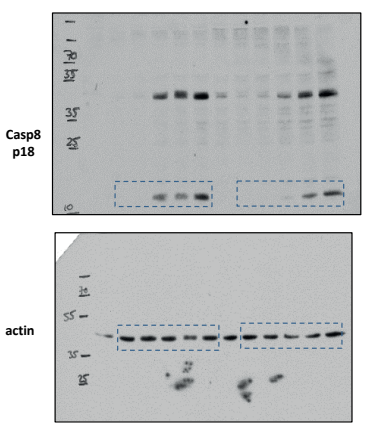

Fig. 6m

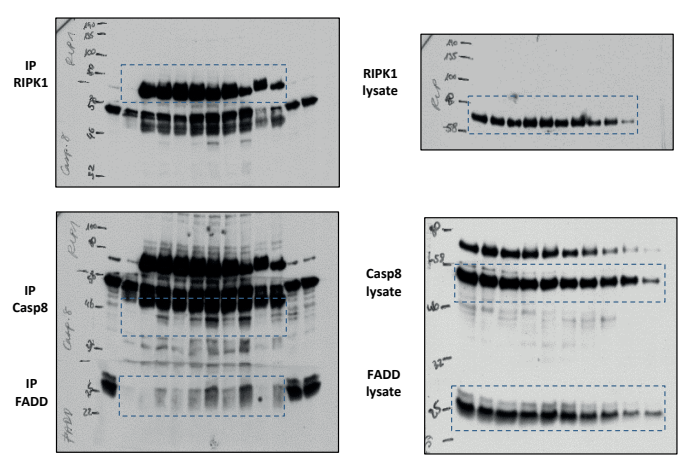

Fig. 6l

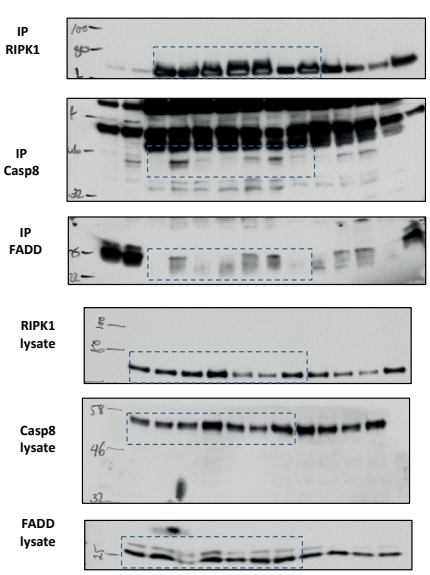

Supplementary Figure 7 Continued

Supplementary Table Legends

Supplementary Table 1 Statistical source data file. The table contains all individual data points for the shown quantitative results and data of independent repeats of representative experiments for Figures 4b, 4c, 4e, 6a, 6c, 6d, 6g, 6h, 6j, 6k, 6n, 6o, and Supplementary Figures S3a, S3b, S3e, S3f, S3h, S4a, S4e, S4g-l, and S5a-c.

Supplementary Table 2 Antibody and Primer data file. The table provides information to all antibodies and primers used in the study.

nature research

Corresponding author(s): NCB-R33092B Ruckdeschel / Gaestel

☐ Initial submission ☒ Revised version ☐ Final submission

Life Sciences Reporting Summary

Nature Research wishes to improve the reproducibility of the work that we publish. This form is intended for publication with all accepted life science papers and provides structure for consistency and transparency in reporting. Every life science submission will use this form; some list items might not apply to an individual manuscript, but all fields must be completed for clarity.

For further information on the points included in this form, see Reporting Life Sciences Research. For further information on Nature Research policies, including our data availability policy, see Authors & Referees and the Editorial Policy Checklist.

Experimental design

1. Sample size

Describe how sample size was determined.

No statistical method was used to predetermine sample size; sample sizes were chosen according to experimental standard procedures for the respective assays.

2. Data exclusions

Describe any data exclusions.

Data were excluded from experiments in which control samples failed to show the expected results.

3. Replication

Describe whether the experimental findings were reliably reproduced.

The shown experiments could successfully and reliably be replicated and reproduced.

4. Randomization

Describe how samples/organisms/participants were allocated into experimental groups.

All samples were randomly allocated to the different experimental groups in which they were then subjected to differential treatment under otherwise identical conditions.

5. Blinding

Describe whether the investigators were blinded to group allocation during data collection and/or analysis.

Blinding was not possible because the samples had to be labeled for the different experimental conditions and experimentors and evaluators were identical.

Note: all studies involving animals and/or human research participants must disclose whether blinding and randomization were used.

6. Statistical parameters

For all figures and tables that use statistical methods, confirm that the following items are present in relevant figure legends (or in the Methods section if additional space is needed).

n/a	Confirmed	
☐	☒	The exact sample size (*n*) for each experimental group/condition, given as a discrete number and unit of measurement (animals, litters, cultures, etc.)
☐	☒	A description of how samples were collected, noting whether measurements were taken from distinct samples or whether the same sample was measured repeatedly
☐	☒	A statement indicating how many times each experiment was replicated
☐	☒	The statistical test(s) used and whether they are one- or two-sided (note: only common tests should be described solely by name; more complex techniques should be described in the Methods section)
☒	☐	A description of any assumptions or corrections, such as an adjustment for multiple comparisons
☐	☒	The test results (e.g. *P* values) given as exact values whenever possible and with confidence intervals noted
☐	☒	A clear description of statistics including central tendency (e.g. median, mean) and variation (e.g. standard deviation, interquartile range)
☐	☒	Clearly defined error bars

See the web collection on statistics for biologists for further resources and guidance.

Software

Policy information about availability of computer code

7. Software

Describe the software used to analyze the data in this study.	Statistics were performed with GraphPad Prism 5 and / or MS Excel 2010

For manuscripts utilizing custom algorithms or software that are central to the paper but not yet described in the published literature, software must be made available to editors and reviewers upon request. We strongly encourage code deposition in a community repository (e.g. GitHub). *Nature Methods* guidance for providing algorithms and software for publication provides further information on this topic.

Materials and reagents

Policy information about availability of materials

8. Materials availability

Indicate whether there are restrictions on availability of unique materials or if these materials are only available for distribution by a for-profit company.	All unique materials used are readily available from the authors.

9. Antibodies

Describe the antibodies used and how they were validated for use in the system under study (i.e. assay and species).	All antibodies used were commercially available with the catalog number details provided in Supplementary Table 2. They are well characterized and were applied according to datasheet information details. Additional controls were included in the present study, wherever necessary.

10. Eukaryotic cell lines

a. State the source of each eukaryotic cell line used.	Information and references to the used cell lines are provided in the manuscript.
b. Describe the method of cell line authentication used.	The cell lines used have not been further authenticated.
c. Report whether the cell lines were tested for mycoplasma contamination.	The cell lines used were tested negative for mycoplasma contamination.
d. If any of the cell lines used are listed in the database of commonly misidentified cell lines maintained by ICLAC, provide a scientific rationale for their use.	No cell lines used in this study were found in the database of commonly misidentified cell lines that is maintained by ICLAC and NCBI Biosample.

Animals and human research participants

Policy information about studies involving animals; when reporting animal research, follow the ARRIVE guidelines

11. Description of research animals

Provide details on animals and/or animal-derived materials used in the study.	Bone marrow cells were derived from male and female mice at the age of 8 to 24 weeks. Handling of the mice complied with all relevant ethical regulations and was approved by the ethics committees of Hannover Medical School and the faculty of medicine at the university of Hamburg.

Policy information about studies involving human research participants

12. Description of human research participants

Describe the covariate-relevant population characteristics of the human research participants.	The study did not involve human research participants.

nature research

NCB-R33092B
Corresponding author(s): Ruckdeschel / Gaestel

☐ Initial submission ☒ Revised version ☐ Final submission

Flow Cytometry Reporting Summary

Form fields will expand as needed. Please do not leave fields blank.

Data presentation

For all flow cytometry data, confirm that:

☒ 1. The axis labels state the marker and fluorochrome used (e.g. CD4-FITC).

☒ 2. The axis scales are clearly visible. Include numbers along axes only for bottom left plot of group (a 'group' is an analysis of identical markers).

☒ 3. All plots are contour plots with outliers or pseudocolor plots.

☒ 4. A numerical value for number of cells or percentage (with statistics) is provided.

Methodological details

5. Describe the sample preparation.	MEF cells were fixed with 2% PFA and permeabilized with 90% methanol before staining with anti-RIPK1 antibodies followed by Alexa-488 labeled secondary antibodies as mentioned in the methods section
6. Identify the instrument used for data collection.	BD Accuri C6
7. Describe the software used to collect and analyze the flow cytometry data.	CFlow Plus (version 1.0.264.15)
8. Describe the abundance of the relevant cell populations within post-sort fractions.	No sorting was employed. The only cells used for flow cytometric analysis were transduced MEF cells already selected for the integrated expression cassette for RIPK1 expression.
9. Describe the gating strategy used.	Cells were gated based on scatter plots, only avoiding debris and aggregates and no extensive gating strategy was used. The flow-cytometry data is presented in the Supplementary Figure 3

Tick this box to confirm that a figure exemplifying the gating strategy is provided in the Supplementary Information. ☒